others showed that AAV8 exhibits strong tropism for neurons in marmoset (Masamizu et al., 2010) and macaque monkey (Dodiya et al., 2010) brains. However, AAV9, another promising neurotropic serotype, has not yet been tested on primate brains.

Several AAV serotypes can transfer genes into neurons via local and retrograde infection. Although local infections from neuronal somata and/or dendrites allow for gene transfer into neurons surrounding the virus administration sites, retrograde infections from axon terminals provide axonal transport of viral genomes. This results in transgene expression in neuronal somata of distal regions that project to the virus administration sites, which could provide strategies for transgene delivery targeted to specific neuronal pathways. For instance, AAV-mediated retrograde gene transfers have been successful in the substantia nigra and in spinal cord motoneurons (Yasuda et al., 2007; Towne et al., 2010). Exploring the infection patterns of AAV8 and AAV9 in primate brains is, therefore, a prerequisite for utilizing these serotypes in a neuronal pathway-specific manner.

The present study initially analyzed the cell tropism of AAV9 in common marmoset and macaque monkey brains. Subsequently, we explored the infection patterns of either AAV8 or AAV9 in the marmoset brain after injection into the striatum to determine the ability of retrograde infection. Moreover, the utilization of this gene transfer strategy was demonstrated by successful application of AAV8 and AAV9 to the geniculocortical pathway of the visual system.

EXPERIMENTAL PROCEDURES

Animals

Five adult, male, common marmosets (*Callithrix jacchus*) and two adult, male, macaque monkeys (*Macaca mulatta* and *Macaca fuscata*) were used for the present study (Table 1). The marmosets were 20–59 months old (230–325 g), and the macaques were 8 years old (9.2 kg) and 7 years old (6.2 kg) at the start of the experiment. All experiments were conducted in accordance with protocols approved by the ethics committee for primate research at the National Center of Neurology and Psychiatry, Japan.

Virus production

Recombinant AAV8 and AAV9 expressing enhanced green fluorescent protein (EGFP) were produced (AAV8-EGFP and AAV9-EGFP, respectively) as previously described (Okada et al., 2005, 2009). The vector plasmid (pAAV-EGFP) contained EGFP cDNA and the woodchuck hepatitis virus post-transcriptional regulatory element (WPRE), which was expressed under control of the CAG promoter, a modified chicken β-actin promoter with a cytomegalovirus immediate early enhancer. AAV8-EGFP and AAV9-EGFP viruses were produced following triple-transfection of HEK293 cells with pAAV-EGFP, an adenoviral helper plasmid pAdeno (Matsushita et al., 1998), and a chimeric helper plasmid encoding either AAV2 rep/AAV8 cap genes or AAV2 rep/AAV9 cap genes (pAAV2-8, pAAV2-9, respectively, gifts from Dr. James M. Wilson) (Gao et al., 2002, 2004), which was mediated by calcium phosphate co-precipitation with active gassing (Okada et al., 2005). At 72 h after transfection, cell suspensions were collected, centrifuged at $300\times g$ for 10 min, and resuspended in 30 ml Tris-buffered saline (100 mM Tris–HCl [pH 8.0], 150 mM NaCl). AAV8-EGFP and AAV9-EGFP viruses were harvested by five-cycle freeze-thawing of the resuspended pellet. The crude viral lysate was initially concentrated by a brief two-tier CsCl gradient centrifugation for 3 h (Okada et al., 2002) and further purified by dual ion-exchange chromatography (Okada et al., 2009). Quantitative polymerase chain reaction of DNase I-treated stocks with plasmid standards determined the final number of AAV8-EGFP and AAV9-EGFP virus particles as 3.0×10^{13} and 9.27×10^{12} vector genomes (vg)/ml, respectively.

Table 1. Injection sites and viral vectors in marmosets and macaques

	Striatum		Primary visual cortex	
Animal	Right	Left	Right	Left
Marmoset A		AAV9		
Marmoset B		AAV9		
Marmoset C		AAV8		
Marmoset D			AAV9	
Marmoset E			AAV9	AAV8
Macaque A				AAV9
Macaque B			AAV8	AAV9

Virus injection

All surgical procedures and virus injections were conducted under aseptic conditions. Animals were initially i.m. anesthetized with 15–22 mg/kg of ketamine (for marmosets) or with 5 mg/kg of ketamine and 0.03 mg/kg of medetomidine (for macaques), followed by intubation and placement in a stereotaxic apparatus. Anesthesia was then maintained with inhalation of isoflurane (1.5–2.5% in oxygen). Saturation of pulse oxygen (SpO_2), heart rate, body temperature, end-tidal CO_2 ($ETCO_2$) and O_2 (ETO_2), isoflurane (ETISO), and fraction of inspired CO_2 ($FiCO_2$), O_2 (FiO_2), and isoflurane (FiISO) were continuously monitored. Following i.m. injection of the antibiotic cefovecin, a small craniotomy (2–3 mm in diameter) was made over the area of interest, and the underlying dura was slit to allow penetration of the virus-containing 10-μl Hamilton syringe connected to a 33 G (45° angle) needle. The viral solution (3 μl) was injected at a rate of 0.25 μl/min at each site. Injection sites were determined with a stereotaxic atlas of the marmoset brain (Yuasa et al., 2010) and the macaque brain (BrainMaps.org, http://brainmaps.org/), respectively. The marmoset injection sites were aimed at the striatum: 12.0 mm anterior from the interaural line, 3.0 mm lateral (L) from the midline and 6.0 mm ventral (V) from the brain surface (Eslamboli et al., 2005), as well as the primary visual cortex: 10.0 mm posterior from the interaural line, 5.0 mm L, and 2.5 mm V (Fritsches and Rosa, 1996). After each injection, the needle was maintained in place for an additional 5 min (striatum) or 15 min (primary visual cortex), and then slowly withdrawn (2 mm/min). The macaque injection sites were aimed at the primary visual cortex. After each injection, the needle was maintained in place for an additional 5 min, and then slowly withdrawn (2 mm/min).

Immunohistochemistry

Procedures were performed as previously described (Nakahira and Yuasa, 2005; Masamizu et al., 2010). At 4 weeks postinjection, animals were deeply anesthetized with a sodium pentobarbital overdose and transcardially perfused with 4% paraformaldehyde in 0.1 M phosphate-buffered saline (PBS, pH 7.4). Brains were removed from the skull and postfixed at 4 °C for 2–3 days using the same fresh fixative. The brains were embedded in 3% agar/PBS and sliced into 100-μm thick coronal sections using a Microslicer (DTK-3000, Dosaka EM, Kyoto, Japan). After 1 h of preincubation with 10% normal goat serum at 4 °C, floating sec-

tions were incubated with primary antibodies in PBS/2% Triton X-100 at 4 °C overnight. Antibodies against the following neuronal or glial marker proteins were used: neuron-specific nuclear protein (NeuN; mouse IgG, 1:500; Cat. No. MAB377, Millipore, Billerica, MA, USA), tyrosine hydroxylase (TH; mouse IgG, 1:1000; Cat. No. T2928, Sigma-Aldrich, St. Louis, MO, USA), glial fibrillary acidic protein (GFAP; rabbit IgG, 1:200; Cat. No. Z0334, Dako, Glostrup, Denmark), and oligodendrocyte transcription factor 2 (Olig2; rabbit IgG, 1:2000 Cat. No. AB9610, Millipore, Billerica, MA, USA). Following PBS rinses, the sections were incubated with secondary antibodies in PBS at 4 °C for 5 h. Secondary antibodies (Alexa goat anti-mouse 594 IgG [1:500; Cat. No. A11005, Molecular Probes, Eugene, OR, USA] or Alexa goat anti-rabbit 594 IgG [1:500; Cat. No. A11012, Molecular Probes, Eugene, OR, USA]), which were directed against the species in which the primary antibody was raised, were used in each case.

Imaging, cell quantification, and statistics

Brain sections were mounted on glass slides with Fluoromount-G (Beckman Coulter, Fullerton, CA, USA). Immunofluorescence and EGFP fluorescence were observed under a confocal laser-scanning microscope (LSM5 Pascal, Zeiss, Oberkochen, Germany) at a resolution of 1024×1024 pixels and one confocal plane. Co-expression of NeuN, GFAP, or Olig2 with EGFP-fluorescence was quantified using ImageJ software (National Institute of Health, Bethesda, MD, USA, http://rsb.info.nih.gov/ij/) with a 40× objective lens. For cell counting analyses, we examined 5–12 microscopic fields in two to four adjacent sections in each case. The number of EGFP-positive cells was statistically analyzed by the chi-square test using JMP8 (SAS Institute, Cary, NC, USA).

Viral transgene detection

Brain slices prepared as in the immunohistochemical analyses (see above) were used for the viral transgene detection assay. Small volumes of tissue were sampled from the injection sites and from regions that contained neuron populations expressing retrograde EGFP labels, under the guidance of EGFP fluorescence by microscopic observation. Extraction and polymerase chain reaction (PCR) amplification of total DNA were performed using the KAPA MG Kit (Cat. No. KK7153, Kapa Biosystems, Woburn, MA, USA). Viral transgenes were detected by PCR using the EGFP (5′-TATATCATGGCCGACAAGCA-3′) and WPRE (5′-CCACATAGCGTAAAAGGAGCA-3′) primers. For internal controls, β-actin DNA was amplified using the primers for β-actin 001 (5′-TCCTGACCCTGAAGTACCCC-3′) and β-actin 002 (5′-GTGGTGGTGAAGCTGTAGCC-3′) (Sasaki et al., 2009).

Thirty-five cycles of PCR were performed (15 s each at 95, 62, and 72 °C) in between an initial denaturation at 95 °C for 3 min and a final elongation at 72 °C for 10 min. PCR products were analyzed by electrophoresis on a 1.2% agarose gel.

RESULTS

Preferential neuronal tropism of AAV9 in marmoset and macaque brains

We have previously shown that AAV8 exhibits a strong tropism for neurons, but not for glia, in the marmoset brain (Masamizu et al., 2010). The present study aimed to determine the tropism of AAV9, which is another promising neurotropic serotype, in the marmoset brain. Recombinant AAV9 expressing the EGFP gene under the CAG promoter (AAV9-EGFP) was generated and stereotaxically injected into the striatum of two marmoset monkeys (Fig. 1A). Four weeks after injection, striatal sections were observed with a confocal microscope. EGFP fluorescence was visible in numerous cell bodies and processes around the injection site (Fig. 1B). Immunohistochemistry revealed that almost all EGFP-positive cells also expressed NeuN (Fig. 1D). Computer-aided cell counting revealed that 99% of EGFP-positive cells also expressed NeuN (Table 2). In contrast, co-expression of EGFP-positive cells with the astrocyte marker GFAP or the oligodendrocyte marker Olig2 was rarely detected (Fig. 1E, F, Table 2). Frequencies of co-localization of cell type-specific markers with EGFP signals were significantly different across cell types ($P<0.0001$, chi-square test; Table 2). Because CAG promoter activity was expected to be ubiquitous across neuronal and glial cell types, these results indicate strong endogenous neuronal tropism of AAV9.

AAV9 neurotropism was also observed in the macaque monkey, the most widely used primate model animal in neuroscience research. AAV9-EGFP was injected into the primary visual cortex of two macaque monkeys. EGFP fluorescence was coexpressed almost exclusively with NeuN, but rarely with glial markers (Fig. 2).

Viral gene transfers to neuronal pathways after the striatum infection

To date, AAV8 and AAV9 infection patterns (local infection from cell bodies/dendrites or retrograde infection from axon terminals) in primate brains have not been elucidated; however, the reciprocal projections between the striatum and substantia nigra offer an appropriate model system for analyzing this. GABAergic neurons in the striatum project to the substantia nigra pars reticulata (SNr), and dopaminergic neurons in the substantia nigra pars compacta (SNc) project to the striatum (Albin et al., 1989; Alexander and Crutcher, 1990; Minamimoto et al., 2009) (Fig. 3B). Therefore, either AAV8-EGFP or AAV9-EGFP was injected into the marmoset striatum, followed by analysis of EGFP expression in the SNr and SNc, ipsilateral to the injection side (Fig. 3A). For both vectors, strong EGFP fluorescence was directly observed in axon terminals in the SNr, as well as in cell bodies of the SNc (Fig. 3C, F). Almost all EGFP-positive cells in the SNc were dopaminergic neurons, as revealed by co-expression of TH (Fig. 3D, G), indicating retrograde EGFP gene transfers after the viral infection in the striatum. We counted the number of EGFP-positive cells among TH-positive neurons to estimate efficacy of retrograde gene transfers. Proportions of EGFP-positive cells among TH-positive neurons were 38% for AAV8 (EGFP-positive/TH-positive: 81/216), and 49% for AAV9 (EGFP-positive/TH-positive: 102/208). In the SNr, high-power confocal images revealed EGFP-positive fibers and varicosities surrounding NeuN-positive cell bodies (Fig. 3E, H). These results suggested that an AAV8-EGFP or AAV9-EGFP injection into the striatum resulted in anterograde transport of transgene products to nerve terminals in the SNr via the striatonigral pathway, as well as retrograde transport of the transgene to cell bodies in the SNc via the nigrostriatal dopaminergic pathway (Fig. 3B).

The striatum receives major projections from the thalamus and the cerebral cortex (Alexander and Crutcher,

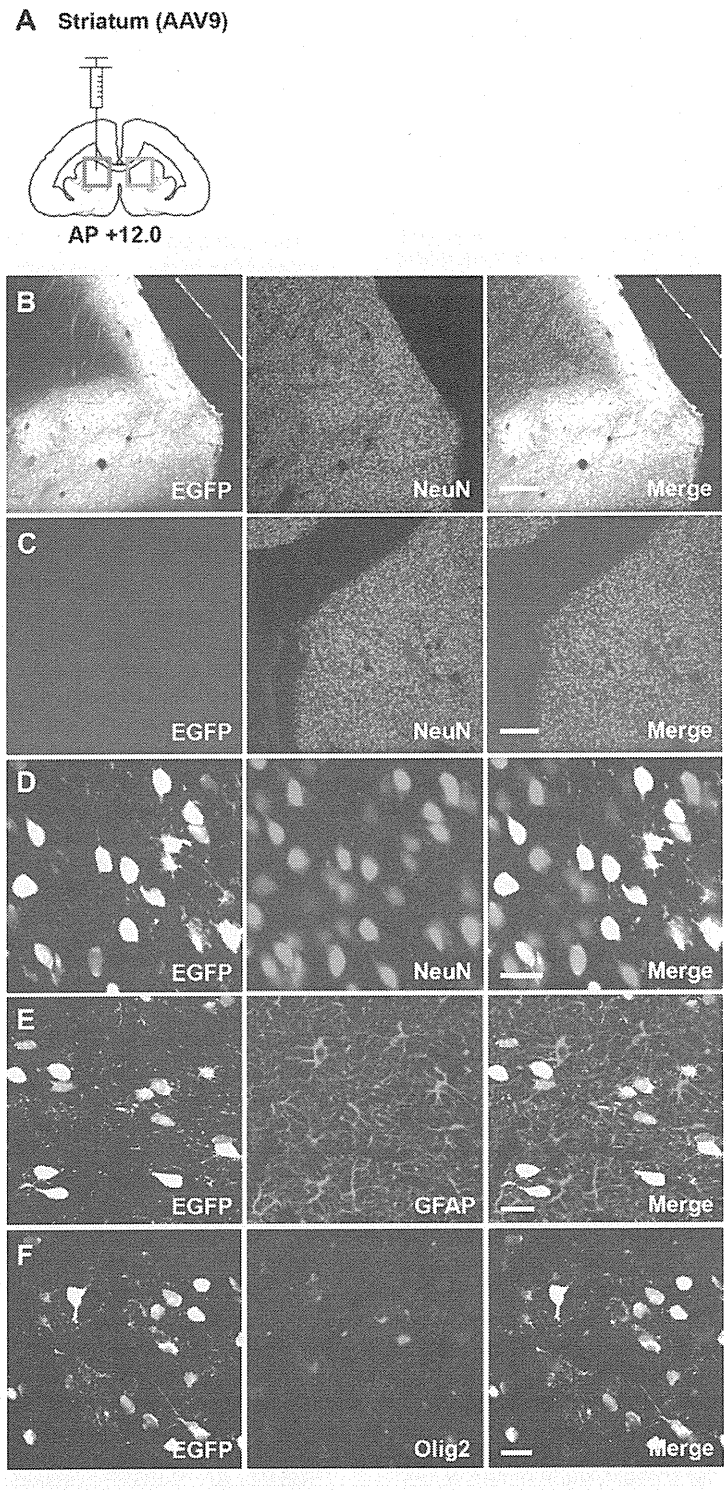

Fig. 1. Efficient gene transfer into neurons of the marmoset striatum using AAV9. (A) The striatal injection site is indicated on a coronal section of the marmoset brain, approximately 12 mm anterior to the interaural line. (B) Low power confocal images corresponding to the red box on the coronal marmoset brain map in (A). Native EGFP fluorescence (left, green), NeuN immunofluorescence signal (center, red), and the merged image (right) are shown. (C) Images of the noninjected control side corresponding to the light-blue box in (A). (D) Confocal images of high-power fields reveal that EGFP-positive cells (green) co-express NeuN (red), as shown by the merged image (yellow). (E, F) EGFP-positive cells (green) rarely co-express GFAP (E; red) or Olig2 (F; red). Bars=200 μm in (B, C) and 20 μm in (D–F). AAV9, adeno-associated virus serotype 9; AP, anteroposterior; EGFP, enhanced green fluorescent protein; GFAP, glial fibrillary acidic protein; NeuN, neuron-specific nuclear protein; Olig2, oligodendrocyte transcription factor 2.

Table 2. Proportion of cells expressing NeuN, GFAP, or Olig2 in EGFP-positive cells in the striatum and primary visual cortex of marmosets following AAV8-EGFP or AAV9-EGFP viral injection

Injection site	Neuron ($NeuN^+/EGFP^+$ cells)	Astrocyte ($GFAP^+/EGFP^+$ cells)	Oligodendrocyte ($Olig2^+/EGFP^+$ cells)
Striatum (AAV8)	98% (484/494)	0% (0/497)	1% (5/500)
Striatum (AAV9)	99% (492/495)	0% (0/500)	1% (3/497)
Primary visual cortex (AAV8)	99% (490/497)	0% (0/502)	1% (3/498)
Primary visual cortex (AAV9)	98% (494/505)	0% (0/493)	1% (5/502)

In all cases, the frequencies of colocalization of cell type-specific markers with EGFP signals are significantly different across cell types ($P<0.0001$, chi-square-test).

1990; Minamimoto et al., 2009). Thus, we also sought retrogradely infected neurons in these regions. We found EGFP expressing neuronal somata in the thalamus probably corresponding to the parafascicular thalamic nucleus (Fig. 4B) (Minamimoto et al., 2009; Yuasa et al., 2010). Neurons expressing EGFP were also found in the frontal and insular cortices at almost the same anterior–posterior level as the striatal injection site (Fig. 4C, D) (Yuasa et al., 2010).

To further confirm retrograde neuronal infections by AAV8 and AAV9, we aimed to detect AAV transgenes in neurons with retrograde EGFP labels. We extracted total DNA from small areas of the frontal/insular cortices and the thalamus where retrograde EGFP labels were observed, and performed PCR using the primers complimentary to a sequence within the AAV construct. For both AAV8 and AAV9, we detected the presence of viral transgenes in the frontal/insular cortices and in the thalamus (Fig. 4E), indicating the viral transgene itself was transported to remote somata after retrograde infections with AAV8 or AAV9.

Local and retrograde gene transfer to the geniculocortical pathway

Gene transfer capabilities of AAV8 and AAV9 were subsequently analyzed in the marmoset visual system. The primary visual cortex (V1) and lateral geniculate nucleus (LGN) constitute reciprocal loops typical for corticothalamic pathways: feedforward projections from the LGN to V1 and feedback projections from the V1 to LGN (Felleman and Van Essen, 1991; Murphy and Sillito, 1996). Either AAV8-EGFP or AAV9-EGFP were injected into the marmoset V1, aiming at the region representing foveal retinotopy, according to previously described electrophysiological mappings (Fritsches and Rosa, 1996). Following injection, EGFP signals were observed across cortical layers at the injection site, and AAV8 and AAV9 neuronal tropisms were confirmed by nearly complete co-expression with NeuN (Table 2). EGFP fluorescence was then detected in the ipsilateral LGN (Fig. 5 for AAV9-EGFP; data not shown for AAV8-EGFP), demonstrating that V1 injection of either AAV8-EGFP or AAV9-EGFP resulted in EGFP expression in the LGN, which was in apparent retinotopic correspondence with the V1 injection site (White et al., 1998) (Fig. 5B). The EGFP labels were apparently restricted to the parvocellular layer (White et al., 1998). In confocal images with high-power magnification, EGFP-positive axons and varicosities were clearly identified (Fig. 5D), suggesting anterograde transport of the transgene products (EGFP) via projections from the V1 to LGN. Neuronal somata also expressed EGFP in the LGN, suggesting retrograde axonal transport of the transgene from the V1 injection site (Fig. 5D). Efficacy of retrograde infections in the LGN were relatively low compared with that in the SNc. Proportions of EGFP-positive cells among NeuN-positive neurons were 15% for AAV8 (EGFP-positive/NeuN-positive: 26/170) and 22% for AAV9 (EGFP-positive/NeuN-positive: 38/173).

DISCUSSION

The present study demonstrated that AAV9 efficiently and selectively infected neurons *in vivo* in the marmoset brain (Fig. 1). This neuronal tropism was similar to that of AAV8, which was shown in our previous study (Masamizu et al., 2010). Results from the present study, in combination with our preliminary results, demonstrate strong AAV8 and AAV9 neurotropism in the brains of macaque monkeys, the most widely used primate animal model in neuroscience research (Fig. 2 for AAV9, data not shown for AAV8). These results suggest that AAV8 and AAV9 exhibit a wide range of neuronal infection across primate species, possibly including humans. To obtain selective transgene expression in neurons, neuron-specific promoters, such as the CaMKII promoter, are used typically. However, neuron-specific promoter activity is often weak and insufficient for effective transgene expression. Endogenous AAV8 and AAV9 tropisms permit efficient and almost exclusive neuronal transgene expression through the use of ubiquitous, strong promoters, such as the CAG promoter, rather than specific, weak promoters.

Recently, Foust et al. (2009, 2010) reported that intravascular injection of AAV9 allows transduction of neurons throughout the brain in newborn mice, as well as in spinal motoneurons of newborn cynomolgus monkeys. In adult mice, however, i.v. delivery of AAV9 results in preferential transduction of astrocytes, rather than neurons. In the present study, AAV9 infected, almost exclusively, neurons in the adult marmoset and macaque brain via direct virus injection into the parenchyma. The discrepancy in cell tropism may be attributed to species differences and/or differences in brain entry: i.v. vs. parenchyma injection. The structure of genomes and the purification procedure of viral particles may also affect cell tropism of AAV vectors. Here, we used conventional single-stranded AAV9 purified with ion-exchange chromatography, whereas Foust et al. used double-stranded, self-complementary AAV9 purified

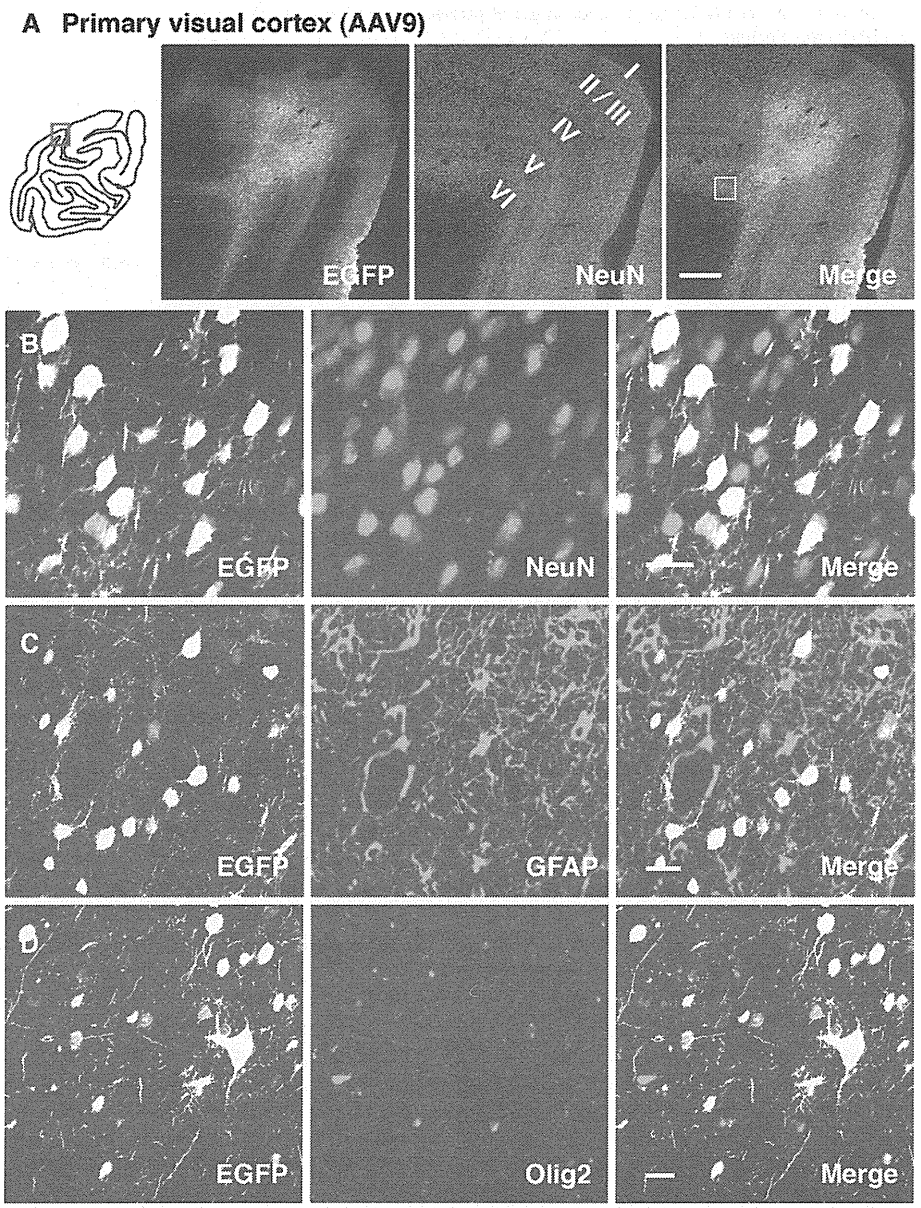

Fig. 2. Gene transfer into neurons of the primary visual cortex of macaque monkeys with AAV9. (A) Low power confocal images at the injection site, approximately corresponding to the red box on a coronal section of the macaque brain map (left). The confocal images reveal prominent EGFP fluorescence around the injection site (green) and NeuN signals (red). (B) Confocal images reveal co-expression of EGFP (green) and NeuN (red), as shown by the merged image (yellow). The view field approximately corresponds to the yellow box on the right panel of (A). (C, D) EGFP-positive cells rarely co-express GFAP (red) or Olig2 (red), as shown by the merged images. Bars=500 μm in (A) and 20 μm in (B–D). The abbreviations are as listed in Fig. 1.

without the use of ion-exchange chromatography. More importantly, results from Foust et al. demonstrated that AAV9 crossed the blood–brain barrier in mice and cynomolgus monkeys, which offers a method for brain-wide gene delivery with less invasiveness, especially for gene therapy applications.

The present study revealed, for the first time, neuronal infection patterns of AAV8 and AAV9 in the primate brain. AAV8, as well as AAV9, exhibited both local and retrograde infection patterns in nigrostriatal, corticostriatal, thalamostriatal and geniculocortical pathways. In the LGN, EGFP labeling was apparently restricted to the parvocellular layers. This observation, together with the observation of a lack of retrograde labeling in other brain regions, which are known to have connections with V1, may suggest that retrograde gene transfer after injection of AAV8 or AAV9 into the V1 are limited to the parvocellular layers of the LGN, although future experiments are required to obtain concrete evidence. For both AAV8 and AAV9, the number of neurons expressing EGFP by retrograde trans-

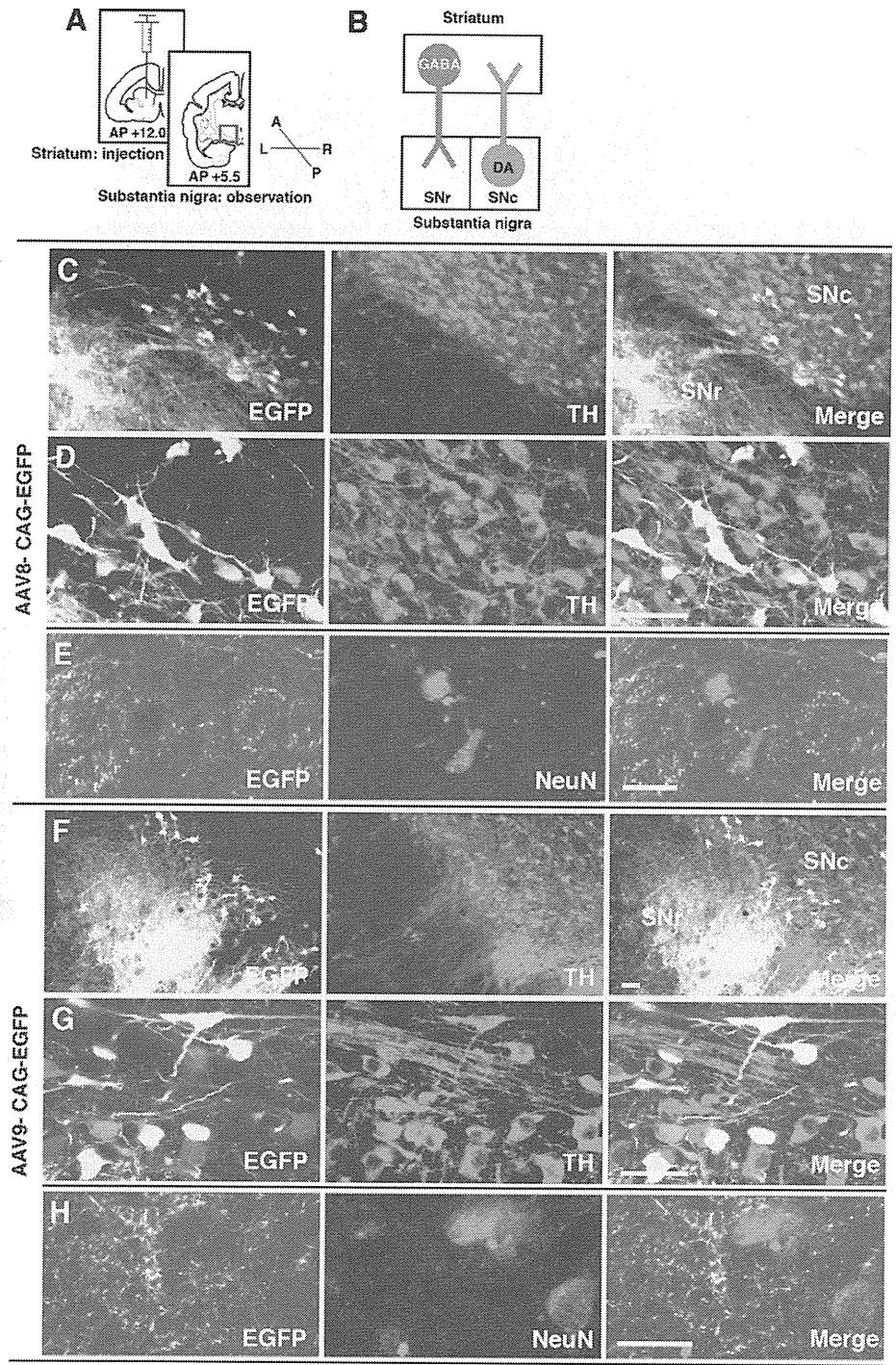

Fig. 3. Local and retrograde gene transfer into the marmoset nigrostriatal pathway with AAV8 and AAV9. (A) Experimental design. EGFP fluorescence is detected in the substantia nigra (red box) following AAV8-EGFP or AAV9-EGFP injection into the striatum. A, anterior; P, posterior; R, right; L, left. (B) Schematic diagram of the nigrostriatal pathway. GABAergic neurons in the striatum (GABA, blue) project to the SNr, and dopaminergic neurons (DA, orange) in the SNc project to the striatum. (C, F) EGFP fluorescence is observed in axon terminals in the SNr, as well as in cell bodies of the SNc following AAV8 (C) or AAV9 (F) injection. (D, G) High-power images of the SNc. EGFP-positive cell bodies (green) co-express TH (red), as shown by the merged images (yellow). (E, H) High-power images of the SNr. EGFP-positive fibers and varicosities (green) are evident around NeuN-positive cell bodies (red). Bars=50 μm in (C, D, F, G) and 20 μm in (E, H). AAV8, adeno-associated virus serotype 8; DA, dopamine; GABA, gamma-aminobutyric acid; SNc, substantia nigra pars compacta; SNr, substantia nigra pars reticulata; TH, tyrosine hydroxylase. Other abbreviations are as listed in Fig. 1.

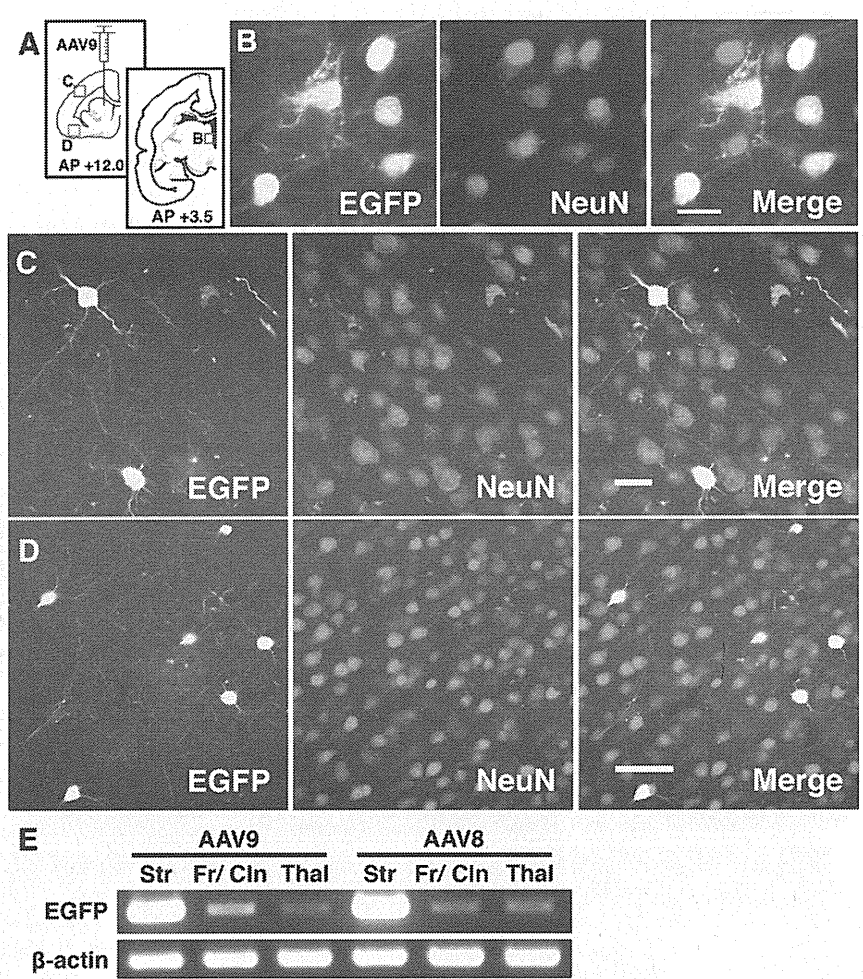

Fig. 4. Retrograde gene transfer into neurons of the frontal/insular cortices and thalamus following AAV9 injection into the striatum. (A) AAV9-EGFP was injected into the striatum at anteroposterior (AP) +12 mm. Retrograde EGFP labels were detected in the thalamus, probably corresponding to the parafascicular thalamic nucleus (B), the frontal cortex (C), and the insular cortex (D). (B–D) Confocal images indicate co-expression of EGFP (green) and NeuN (red) in the thalamus (B), the frontal cortex (C), and the insular cortex (D), as shown in the merged images (yellow). (E) Polymerase chain reaction (PCR) analyses reveal the presence of viral transgene (EGFP) not only in the striatal local infection site (Str), but also in the frontal/insular cortices (Fr/Cln) and the thalamus (Thal) in which cell bodies with retrograde EGFP fluorescence were observed. Bars=20 μm in (B, C) and 50 μm in (D). PCR, polymerase chain reaction. Other abbreviations are as listed in Fig. 1.

fer was modest in the substantia nigra and relatively small in the LGN. Transgene expression was examined at 4 weeks after viral injection; however, the time frame may be insufficient for acquiring full transgene expression in the somata via retrograde transport. In general, AAV-mediated transgene expression persists for long periods (more than a year), and long-term expression would allow for improved efficiency of neuronal transgene expression via retrograde AAV transport.

In the present study, we conducted PCR analyses and confirmed the presence of viral transgenes in the neuronal somata following retrograde infections of either AAV8 or AAV9. These results prove that the genome of AAV8 or AAV9 itself is transported to the soma after retrograde infection at the axon terminal in the brain. This probable mechanism has been demonstrated in several other AAV serotypes, such as AAV1, AAV2, and AAV6 (Kaspar et al., 2002; Hollis et al., 2008; Towne et al., 2010).

A number of neuroscience studies have demonstrated the roles of hierarchical and interconnected structures of the brain in terms of information processing for cognition and behavior (Felleman and Van Essen, 1991; Murphy and Sillito, 1996; Nishimura et al., 2007; Bostan et al., 2010). Retrograde neuronal delivery of molecular tools through the use of AAV8 or AAV9 vectors could provide methods for analyzing hierarchical information processing in the brain. For example, injection of recombinant AAV8 or AAV9 expressing transgenes encoding optogenetic tools into a given brain region could lead to transgene neuronal delivery with direct projections to the injected site, thereby allowing for experimental *in vivo* manipulation of neuronal inputs to the injected brain area. Therefore, transgene

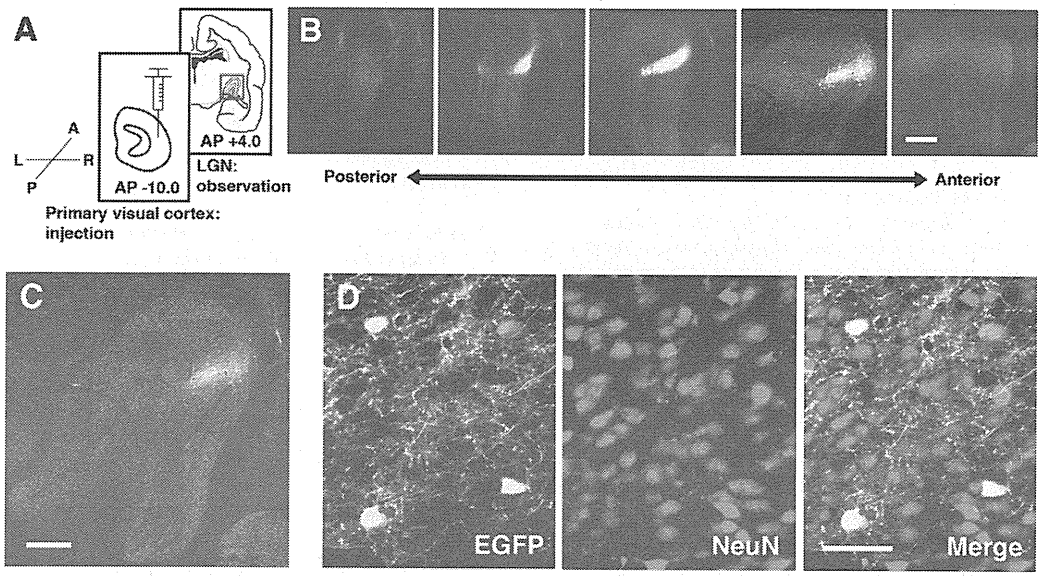

Fig. 5. Local and retrograde gene transfer into the marmoset geniculocortical pathway with AAV9. (A) Experimental design. EGFP expression is visible in the LGN (red box) following injection of AAV9-EGFP into the primary visual cortex. (B) Confocal images of EGFP fluorescence (green) and NeuN expression (red) in coronal sections of the LGN, approximately 3.4–4.2 mm anterior to the interaural line. (C) Representative coronal section of the LGN around the center of EGFP expression (green) overlaid on NeuN signals (red). Approximately 4.0 mm anterior to the interaural line. (D) High-power confocal images show EGFP-positive cell bodies, axons and varicosities (green) in the LGN. EGFP-positive cell bodies co-express NeuN (red), as shown by the merged image (yellow). Bars=500 μm in (B, C) and 50 μm in (D). LGN, lateral geniculate nucleus. Remaining abbreviations are as listed in Fig. 1.

delivery into primate brains via AAV8 and AAV9 vectors could facilitate studies focused on circuit-based principles of brain function by utilizing high-infection efficiencies, as well as neuronal infection patterns.

CONCLUSIONS

Results from the present study, in combination with our previous study, revealed that AAV8 and AAV9 exhibited strong endogenous tropism for neurons in primate brains. The present results further demonstrated that these AAV serotypes can infect neurons both locally and retrogradely. These infection patterns allow transgene delivery to local neurons surrounding virus-injection sites via local infection from somata/dendrites, as well as to distal neurons that project to virus-injection sites via retrograde infections from axon terminals.

Acknowledgments—We thank Dr. James M. Wilson for providing helper plasmids pAAV2-8 (originally described as p5E18-VD2/8) and pAAV2-9. This study was supported by the JSPS Research Fellowship for Young Scientists (Y.M.) and by PRESTO, JST (K.N.). All authors declare no conflict of interest.

REFERENCES

Albin RL, Young AB, Penney JB (1989) The functional anatomy of basal ganglia disorders. Trends Neurosci 12:366–375.

Alexander GE, Crutcher MD (1990) Functional architecture of basal ganglia circuits: neural substrates of parallel processing. Trends Neurosci 13:266–271.

Bostan AC, Dum RP, Strick PL (2010) The basal ganglia communicate with the cerebellum. Proc Natl Acad Sci U S A 107:8452–8456.

Broekman ML, Comer LA, Hyman BT, Sena-Esteves M (2006) Adeno-associated virus vectors serotyped with AAV8 capsid are more efficient than AAV-1 or -2 serotypes for widespread gene delivery to the neonatal mouse brain. Neuroscience 138: 501–510.

Chan AW, Chong KY, Martinovich C, Simerly C, Schatten G (2001) Transgenic monkeys produced by retroviral gene transfer into mature oocytes. Science 291:309–312.

Dodiya HB, Bjorklund T, Stansell J, III, Mandel RJ, Kirik D, Kordower JH (2010) Differential transduction following basal ganglia administration of distinct pseudotyped AAV capsid serotypes in nonhuman primates. Mol Ther 18:579–587.

Eslamboli A, Georgievska B, Ridley RM, Baker HF, Muzyczka N, Burger C, Mandel RJ, Annett L, Kirik D (2005) Continuous low-level glial cell line-derived neurotrophic factor delivery using recombinant adeno-associated viral vectors provides neuroprotection and induces behavioral recovery in a primate model of Parkinson's disease. J Neurosci 25:769–777.

Felleman DJ, Van Essen DC (1991) Distributed hierarchical processing in the primate cerebral cortex. Cereb Cortex 1:1–47.

Foust KD, Nurre E, Montgomery CL, Hernandez A, Chan CM, Kaspar BK (2009) Intravascular AAV9 preferentially targets neonatal neurons and adult astrocytes. Nat Biotechnol 27:59–65.

Foust KD, Wang X, McGovern VL, Braun L, Bevan AK, Haidet AM, Le TT, Morales PR, Rich MM Burghes AH, Kaspar BK (2010) Rescue of the spinal muscular atrophy phenotype in a mouse model by early postnatal delivery of SMN. Nat Biotechnol 28:271–274.

Fritsches KA, Rosa MG (1996) Visuotopic organisation of striate cortex in the marmoset monkey (Callithrix jacchus). J Comp Neurol 372:264–282.

Gao G, Vandenberghe LH, Alvira MR, Lu Y, Calcedo R, Zhou X, Wilson JM (2004) Clades of Adeno-associated viruses are widely disseminated in human tissues. J Virol 78:6381–6388.

Gao GP, Alvira MR, Wang L, Calcedo R, Johnston J, Wilson JM (2002) Novel adeno-associated viruses from rhesus monkeys

as vectors for human gene therapy. Proc Natl Acad Sci U S A 99:11854–11859.

Han X, Qian X, Bernstein JG, Zhou HH, Franzesi GT, Stern P, Bronson RT, Graybiel AM, Desimone R, Boyden ES (2009) Millisecond-timescale optical control of neural dynamics in the nonhuman primate brain. Neuron 62:191–198.

Hollis ER, II, Kadoya K, Hirsch M, Samulski RJ, Tuszynski MH (2008) Efficient retrograde neuronal transduction utilizing self-complementary AAV1. Mol Ther 16:296–301.

Kaplitt MG, Leone P, Samulski RJ, Xiao X, Pfaff DW, O'Malley KL, During MJ (1994) Long-term gene expression and phenotypic correction using adeno-associated virus vectors in the mammalian brain. Nat Genet 8:148–154.

Kaspar BK, Erickson D, Schaffer D, Hinh L, Gage FH, Peterson DA (2002) Targeted retrograde gene delivery for neuronal protection. Mol Ther 5:50–56.

Masamizu Y, Okada T, Ishibashi H, Takeda S, Yuasa S, Nakahara K (2010) Efficient gene transfer into neurons in monkey brain by adeno-associated virus 8. Neuroreport 21:447–451.

Matsushita T, Elliger S, Elliger C, Podsakoff G, Villarreal L, Kurtzman GJ, Iwaki Y, Colosi P (1998) Adeno-associated virus vectors can be efficiently produced without helper virus. Gene Ther 5:938–945.

Minamimoto T, Hori Y, Kimura M (2009) Roles of the thalamic CM-PF complex-Basal ganglia circuit in externally driven rebias of action. Brain Res Bull 78:75–79.

Murphy PC, Sillito AM (1996) Functional morphology of the feedback pathway from area 17 of the cat visual cortex to the lateral geniculate nucleus. J Neurosci 16:1180–1192.

Nakahara K, Adachi Y, Osada T, Miyashita Y (2007) Exploring the neural basis of cognition: multi-modal links between human fMRI and macaque neurophysiology. Trends Cogn Sci 11:84–92.

Nakahira E, Yuasa S (2005) Neuronal generation, migration, and differentiation in the mouse hippocampal primoridium as revealed by enhanced green fluorescent protein gene transfer by means of in utero electroporation. J Comp Neurol 483:329–340.

Nishimura Y, Onoe H, Morichika Y, Perfiliev S, Tsukada H, Isa T (2007) Time-dependent central compensatory mechanisms of finger dexterity after spinal cord injury. Science 318:1150–1155.

Okada T, Nomoto T, Yoshioka T, Nonaka-Sarukawa M, Ito T, Ogura T, Iwata-Okada M, Uchibori R, Shimazaki K, Mizukami H, Kume A, Ozawa K (2005) Large-scale production of recombinant viruses by use of a large culture vessel with active gassing. Hum Gene Ther 16:1212–1218.

Okada T, Nonaka-Sarukawa M, Uchibori R, Kinoshita K, Hayashita-Kinoh H, Nitahara-Kasahara Y, Takeda S, Ozawa K (2009) Scalable purification of adeno-associated virus serotype 1 (AAV1) and AAV8 vectors, using dual ion-exchange adsorptive membranes. Hum Gene Ther 20:1013–1021.

Okada T, Shimazaki K, Nomoto T, Matsushita T, Mizukami H, Urabe M, Hanazono Y, Kume A, Tobita K, Ozawa K, Kawai N (2002) Adeno-associated viral vector-mediated gene therapy of ischemia-induced neuronal death. Methods Enzymol 346:378–393.

Passingham R (2009) How good is the macaque monkey model of the human brain? Curr Opin Neurobiol 19:6–11.

Sasaki E, Suemizu H, Shimada A, Hanazawa K, Oiwa R, Kamioka M, Tomioka I, Sotomaru Y, Hirakawa R, Eto T, Shiozawa S, Maeda T, Ito M, Ito R, Kito C, Yagihashi C, Kawai K, Miyoshi H, Tanioka Y, Tamaoki N, Habu S, Okano H, Nomura T (2009) Generation of transgenic non-human primates with germline transmission. Nature 459:523–527.

Tan EM, Yamaguchi Y, Horwitz GD, Gosgnach S, Lein ES, Goulding M, Albright TD, Callaway EM (2006) Selective and quickly reversible inactivation of mammalian neurons in vivo using the Drosophila allatostatin receptor. Neuron 51:157–170.

Taymans JM, Vandenberghe LH, Haute CV, Thiry I, Deroose CM, Mortelmans L, Wilson JM, Debyser Z, Baekelandt V (2007) Comparative analysis of adeno-associated viral vector serotypes 1, 2, 5, 7, and 8 in mouse brain. Hum Gene Ther 18:195–206.

Towne C, Schneider BL, Kieran D, Redmond DE, Jr, Aebischer P (2010) Efficient transduction of non-human primate motor neurons after intramuscular delivery of recombinant AAV serotype 6. Gene Ther 17:141–146.

White AJ, Wilder HD, Goodchild AK, Sefton AJ, Martin PR (1998) Segregation of receptive field properties in the lateral geniculate nucleus of a New-World monkey, the marmoset Callithrix jacchus. J Neurophysiol 80:2063–2076.

Yasuda T, Miyachi S, Kitagawa R, Wada K, Nihira T, Ren YR, Hirai Y, Ageyama N, Terao K, Shimada T, Takada M, Mizuno Y, Mochizuki H (2007) Neuronal specificity of alpha-synuclein toxicity and effect of Parkin co-expression in primates. Neuroscience 144:743–753.

Yuasa S, Nakamura K, Kohsaka S (2010) Stereotaxic atlas of the marmoset brain with immunohistochemical architecture and MRI Images. National Institute of Neuroscience, National Center of Neurology and Psychiatry, Tokyo, Japan.

Zhang F, Wang LP, Brauner M, Liewald JF, Kay K, Watzke N, Wood PG, Bamberg E, Nagel G, Gottschalk A, Deisseroth K (2007) Multimodal fast optical interrogation of neural circuitry. Nature 446:633–639.

(Accepted 28 June 2011)
(Available online 18 July 2011)

Journal of Neurochemistry JNC

JOURNAL OF NEUROCHEMISTRY | 2011 | 116 | 1122–1137 doi: 10.1111/j.1471-4159.2010.07167.x

SynArfGEF is a guanine nucleotide exchange factor for Arf6 and localizes preferentially at post-synaptic specializations of inhibitory synapses

Masahiro Fukaya,* Akifumi Kamata,* Yoshinobu Hara,* Hideaki Tamaki,* Osamu Katsumata,* Naoki Ito,†,‡ Shin'ichi Takeda,† Yutaka Hata,§ Tatsuo Suzuki,¶ Masahiko Watanabe,** Robert J. Harvey†† and Hiroyuki Sakagami*

*Department of Anatomy, Kitasato University School of Medicine, Sagamihara, Japan

†Department of Molecular Therapy, National Institute of Neuroscience, National Center of Neurology and Psychiatry, Kodaira, Japan

‡Department of Biological Information, Tokyo Institute of Technology, Nagatsuta, Yokohama, Japan

§Department of Medical Biochemistry, Graduate School of Medicine, Tokyo Medical and Dental University, Bunkyo-ku, Tokyo, Japan

¶Department of Neuroplasticity, Institute on Aging and Adaptation, Shinshu University Graduate School of Medicine, Matsumoto, Japan

**Department of Anatomy, Hokkaido University School of Medicine, Sapporo, Japan

††Department of Pharmacology, The School of Pharmacy, London, UK

Abstract

SynArfGEF, also known as BRAG3 or IQSEC3, is a member of the brefeldin A-resistant Arf-GEF/IQSEC family and was originally identified by screening for mRNA species associated with the post-synaptic density fraction. In this study, we demonstrate that synArfGEF activates Arf6, using Arf pull down and transferrin incorporation assays. Immunohistochemical analysis reveals that synArfGEF is present in somata and dendrites as puncta in close association with inhibitory synapses, whereas immunoelectron microscopic analysis reveals that synArfGEF localizes preferentially at post-synaptic specializations of symmetric synapses. Using yeast two-hybrid and pull down assays, we show that synArfGEF is able to bind utrophin/dystrophin and S-SCAM/MAGI-2 scaffolding proteins that localize at inhibitory synapses. Double immunostaining reveals that synArfGEF co-localizes with dystrophin and S-SCAM in cultured hippocampal neurons and cerebellar cortex, respectively. Both β-dystroglycan and S-SCAM were immunoprecipitated from brain lysates using anti-synArfGEF IgG. Taken together, these findings suggest that synArfGEF functions as a novel regulator of Arf6 at inhibitory synapses and associates with the dystrophin-associated glycoprotein complex and S-SCAM.

Keywords: ADP-ribosylation factor 6, dystrophin, gephyrin, PDZ domain, post-synaptic density.

J. Neurochem. (2011) **116**, 1122–1137.

Chemical synapses are specialized sites of the communication between neurons where information is processed and integrated. Electron microscopy has allowed morphological

Received November 24, 2010; revised manuscript received December 8, 2010; accepted December 9, 2010.

Address correspondence and reprint requests to Hiroyuki Sakagami, MD, PhD, Department of Anatomy, Kitasato University School of Medicine, Sagamihara, Kanagawa 252-0374, Japan.
E-mail: sakagami@med.kitasato-u.ac.jp

Abbreviations used: Arf, ADP ribosylation factor; BRAG, brefeldin A-resistant Arf-GEF; DGC, dystrophin-associated glycoprotein complex; $GABA_AR$, $GABA_A$ receptor; GAP, GTPase-activating protein; GEF, guanine nucleotide exchange factor; GGA1, Golgi-localizing, γ-adaptin ear homology domain, Arf-binding protein 1; GST, glutathione S-transferase; HA, hemagglutinin; IRSP, insulin receptor tyrosine kinase substrate of 53 kDa; MAGI, membrane-associated guanylate kinase with inverted orientation; PDZ, PSD-95/Discs large/Zona occludens 1; PSD, post-synaptic density; SDS, sodium dodecyl sulfate; SDS–PAGE, SDS–polyacrylamide gel electrophoresis; S–SCAM, synaptic scaffolding molecule; synArfGEF(Po), potential synaptic Arf-GEF; VGAT, vesicular γ-aminobutyric acid transporter.

classification of synapses into asymmetric and symmetric types (Gray 1959). Asymmetric synapses, also called Gray's type I synapses, are usually excitatory, use glutamate as a neurotransmitter and are formed on dendritic spines. They feature a prominent electron-dense thickening at the cytoplasmic surface of the post-synaptic membrane called a post-synaptic density (PSD). Intensive proteomic and molecular cloning analyses have identified the molecular components of excitatory PSDs, which consist of glutamate receptors, cell adhesion molecules, scaffolding and adaptor proteins, cytoskeletal proteins, and signaling molecules including regulators of small GTPases, protein kinases and phosphatases (Scannevin and Huganir 2000).

By contrast, symmetric synapses, also called Gray's type II synapses, are usually inhibitory, use either GABA or glycine as neurotransmitters and are mainly formed on dendritic shafts and cell bodies. The PSD at inhibitory synapses is less electron-dense, having a similar size to the active zone on the pre-synaptic membrane. Our understanding of the molecular organization of inhibitory synapses lags behind that of excitatory PSDs, in part because of the difficulty of purification of inhibitory PSDs. Several components such as gephyrin and dystrophin-associated glycoprotein complex (DGC) are found to localize selectively at post-synaptic specializations of inhibitory synapses and are proposed to be essential for the formation and maintenance of inhibitory synapses. Gephyrin is a 93-kDa peripheral membrane protein that was originally co-purified with glycine receptors (Pfeiffer *et al.* 1982). Several lines of evidence indicate that gephyrin is essential for the post-synaptic clustering of glycine receptors (Kirsch *et al.* 1993; Feng *et al.* 1998) and α2- and γ2-subunit containing $GABA_A$ receptors ($GABA_A$Rs) (Essrich *et al.* 1998). Gephyrin functions as synaptic scaffold and regulator of receptor trafficking by interacting with various membrane, signaling, cytoskeletal, and trafficking proteins (Kneussel and Betz 2000; Fritschy *et al.* 2008). Among gephyrin-interacting proteins, collybistin, a guanine nucleotide exchange factor (GEF), was originally considered to govern synaptic gephyrin localization, because collybistin splice variants lacking a *src* homology 3 domain can recruit gephyrin from intracellular aggregates to submembrane clusters in heterologous transfection systems (Kins *et al.* 2000; Harvey *et al.* 2004). However, most isoforms *in vivo* harbor an Src homology 3 domain, which mediates activation of collybistin-mediated gephyrin clustering by neuroligin 2 (Poulopoulos *et al.* 2009). Curiously, studies with collybistin-deficient mice have revealed that collybistin is only essential for gephyrin-dependent clustering of specific subsets of $GABA_A$Rs in the hippocampus and amygdala (Papadopoulos *et al.* 2007), suggesting that other clustering mechanisms must operate at inhibitory synapses. On the other hand, the DGC is a large multiprotein complex that links the extracellular matrix to the cytoskeleton. Several components of the DGC, including α- and β-dystroglycan, dystrophin, and β-dystrobrevin were shown to selectively localize to inhibitory synapses on neuronal somata and dendrites (Knuesel *et al.* 1999; Brunig *et al.* 2002; Levi *et al.* 2002; Grady *et al.* 2006). A study with dystrophin mutant *mdx* mice also demonstrated that a lack of dystrophin reduced the clustering of $GABA_A$R α1 and α2 subunits in the hippocampus and cerebellum (Knuesel *et al.* 1999), suggesting that gephyrin-independent mechanisms also regulate the clustering of $GABA_A$R α1 and α2 subunits.

SynArfGEF(Po), named as a *potential* synaptic guanine nucleotide exchange factor (GEF) for the ADP ribosylation factor (Arf) family of small GTPases, was originally identified by screening for mRNA species associated with the PSD fraction (Inaba *et al.* 2004). SynArfGEF(Po) contains an N-terminal coiled-coil motif, a calmodulin-binding IQ-like motif, central Sec7 domain and pleckstrin homology domain and a C-terminal type I PSD-95/Disc large/Zonula occludens 1 (PDZ)-binding motif (Inaba *et al.* 2004). All Arf-GEFs contain a Sec7 domain, an approximately 200-amino acid protein module that is critical for the catalysis of GDP-GTP exchange on Arf GTPases. SynArfGEF(Po) belongs to the brefeldin A-resistant Arf-GEF (BRAG)/IQSEC subfamily of Arf-GEFs based on the phylogenic classification of Sec7 domains (Cox *et al.* 2004). The Arf family comprises six structurally related members (Arf1-6) that play an essential role in membrane trafficking and cytoskeletal rearrangements (D'Souza-Schorey and Chavrier 2006). Among six Arf members, Arf6 is the most divergent in terms of structure, localizes at plasma membrane and endosomes, and regulates recycling of the plasma membrane and peripheral actin cytoskeleton. In neurons, Arf6 is implicated in the formation and maintenance of dendritic spines (Choi *et al.* 2006), the branching of axons and dendrites (Hernandez-Deviez *et al.* 2002, 2004), exocytosis and endocytosis of synaptic vesicles (Vitale *et al.* 2002; Krauss *et al.* 2003) and receptor internalization (Delaney *et al.* 2002; Krauss *et al.* 2003; Claing 2004; Houndolo *et al.* 2005). SynArfGEF(Po) mRNA is expressed widely in the rat brain and localized at dendrites as well as cell bodies, suggesting activity-dependent local translation (Inaba *et al.* 2004). Although synArfGEF(Po) protein shows a punctate appearance in cell bodies and dendrites of cultured neurons, its subcellular localization has not been characterized in detail to date.

To obtain a better understanding of the functional significance of synArfGEF(Po), we first demonstrated its ability to activate Arf6 and therefore renamed it synArfGEF. Next, we examined the immunohistochemical localization of synArfGEF in the mouse brain. Intriguingly, synArfGEF exhibited somatodendritic localization with a high selectivity for post-synaptic specializations of inhibitory synapses. We further demonstrated the ability of synArfGEF to interact with utrophin/dystrophin and synaptic scaffolding molecule

(S-SCAM) by yeast two-hybrid and pull down assays. These findings indicate that synArfGEF is a novel signaling component at inhibitory post-synaptic sites.

Materials and methods

All animal protocols were approved by the Animal Experimentation and Ethics Committee of the Kitasato University School of Medicine and followed the guidelines of the National Institutes of Health.

Vectors

Mammalian expression vectors for synArfGEF (pCAGGS-FLAG-synArfGEF) and GEP100/BRAG2 (pCAGGS-FLAG-GEP100) were made by amplifying the coding regions of rat synArfGEF and mouse GEP100 using PCR with primers containing *Eco*RI restriction sites (underlined) as follows: sense, 5′-GAATTCATGGAGAGCCTGC TGGAGAACCCGG-3′ and antisense, 5′-GAATTCCTACACCAGG CTCCTGGAGCCACTG-3′ for synArfGEF; sense, 5′-GAATTCAT GCTAGAACGCAAGTATGGGGGAC-3′ and antisense, 5′-GAAT TCTTAGGAGCACAGCACTGGAGGCTG-3′ for GEP100. After subcloning into pGEM-T Easy (Promega, Madison, WI, USA), the cDNA fragments were digested with *Eco*RI and ligated into the same restriction site of pCAGGS-FLAG (Niwa *et al.* 1991; Sakagami *et al.* 2005). A mammalian expression vector for IQ-ArfGEF/BRAG1, pCAGGS-FLAG-IQ-ArfGEF/BRAG1, was described previously (Sakagami *et al.* 2008). The expression vectors for S-SCAM [pCIneoMyc S-SCAM (1–1277), (1–301), (295–578), (423–578)] were described previously (Sumita *et al.* 2007). The expression vectors for C-terminally hemagglutinin (HA) epitope-tagged Arf1 and Arf6 in pcDNA3 (Hosaka *et al.* 1996) were kindly provided by Dr Kazuhisa Nakayama (Kyoto University). The expression vector for C-terminally FLAG-tagged Arf6(Q67L) mutant in pCAGGS-neo (Tanabe *et al.* 2005) was kindly provided by Dr Masanobu Satake (Tohoku University).

For Arf pull down assays, the bacterial expression vector containing the GAT domain of Golgi-localizing, γ-adaptin ear homology domain, Arf-binding protein 1 (GGA1) (Shinotsuka *et al.* 2002) was kindly provided by Dr Kazuhisa Nakayama (Kyoto University).

For pMAL-SXN, a bacterial expression vector that has the same reading frame for the *Sal*I cloning site as that of pGEX4T-2 (GE Healthcare, Piscataway, NJ, USA), oligonucleotides containing *Sal*I, *Xho*I and *Not*I sites (5′-AATTGTCGACTCGAGCGGCCGCTGCA-3′ and 5′-GCGGCCGCTCGAGTCGAC-3′) were annealed and ligated into the *Eco*RI and *Pst*I sites of pMAL-c2 (New England Biolabs, Beverly, MA, USA). To prepare antigens for immunization and affinity purification, the N-terminal region (amino acids 1–293) of rat synArfGEF, the entire coding region of mouse gephyrin, the region between PDZ1 and PDZ2 domain of rat S-SCAM (amino acids 510–570), the region containing 13th and 14th spectrin repeats of mouse utrophin (amino acids 1761–2101) were amplified by PCR with the following primers containing a *Sal*I site (underlined) in sense primers and a stop codon (small letters) in antisense primers: 5′-GTCGACCATGGAGAGCCTGCTGGAGAACCCGG-3′ and 5′-ctaTAGGTCAAGGGAGAGTTCGTACTC-3′ for synArfGEF; GT CGACCATGGCGACCGAGGGAATGATCCTCAC-3′ and tcaTAG CCGTCCAATGACCATGACATC-3′ for gephyrin; 5′-GTCGAC CTGTCGTGGCTACCCTTTGCCCTTTG and 5′ctaGTGCAA AGAATGAGGTGGCCGGTCTG-3′ for S-SCAM; 5′-GTCGAC GACCCTGCTGGAACTGTTCAAGCTGC-3′ and 5′-ttaCGTTAA CCAGCAGGTGACCTCATCTAGCC-3′ for utrophin. After subcloning into pGEM-T Easy, the cDNA fragments were digested with *Sal*I and *Not*I and ligated into the same restriction sites of pGEX4T-2 and pMAL-SXN.

For *in vitro* binding assays, the C-terminal region of rat synArfGEF (amino acids 1122–1194) was amplified by PCR with primers containing a *Sal*I site (underlined) (5′-GTCGACCAT GGAGCCCCTGCTGAGCCAGGCTC-3′ and 5′-CTACACCAG GCTCCTGGAGCCACTG-3′). After subcloning into pGEM-T Easy, the cDNA fragment digested with *Sal*I and *Not*I was ligated into the same restriction sites of pGEX4T-2. The C-terminal regions of utrophin corresponding to amino acids 2961–3429, 2691–3058, and 2691–2843 and dystrophin corresponding to amino acids 2937–3685 were amplified by PCR using the primer combinations listed in Table S1 and ligated into pGEM-T Easy. The inserts were digested with *Sal*I and *Not*I and ligated into the same sites of pGEX4T-2.

To construct bait vectors for yeast two-hybrid assays, the C-terminal regions of synArfGEF shown in Fig. 7b were amplified by PCR with primer combinations listed in Table S1 and rat synArfGEF cDNA as a template. After ligation into pGEM-T Easy, the inserts were ligated into *Sal*I and *Not*I sites of pDBLeu (Invitrogen Corp., Carlsbad, CA, USA) downstream and in frame with the GAL4 DNA binding domain. For pDBLeu-syn-ArfGEF(PPPPY → PPAPA), mutations were introduced in a PY motif at the C-terminus of synArfGEF using the PrimeSTAR mutation basal kit (Takara, Tokyo, Japan) with pDBLeu-syn-ArfGEF(1122–1194) and mutagenesis oligonucleotides (sense, 5′-CCCCAGCCCCAGCCAACCACCCTCACCAGTT-3′; antisense, 5′-GTGGTTGGCTGGGGCTGGGGGTGGGGGCAGTGG-3′). To construct prey vectors encoding truncated mutants of utrophin and dystrophin as shown in Fig 6a, PCR was carried out with the primer combinations listed in Table S1. After ligation into pGEM-T Easy, the inserts digested with *Sal*I and *Not*I were ligated into the same sites of pPC86. All inserts created in this study were confirmed by Sanger DNA sequencing.

Arf Pull down assay

The GEF activity of synArfGEF was examined by Arf pull down assays with GGA1 as described previously (Takatsu *et al.* 2002; Sakagami *et al.* 2006). COS-7 cells were transfected with pcDNA3-Arf1-HA or pcDNA3-Arf6-HA in the presence or absence of pCAGGS-FLAG-synArfGEF using Lipofectamine 2000 (Invitrogen). Cells were lysed in a buffer containing 50 mM Tris–HCl (pH 7.5), 100 mM NaCl, 2 mM $MgCl_2$, 0.1% sodium dodecyl sulfate (SDS), 0.5% sodium deoxycholate, 1% Triton X-100, 10% glycerol and a cocktail of protease inhibitors (Complete Mini™, Roche, Mannheim, Germany). After centrifugation, the supernatants were incubated with 40 μg of glutathione S-transferase (GST)-GGA1 fusion protein immobilized on glutathione-Sepharose 4B (GE Healthcare) for 1 h at 4°C. The precipitates and lysates were separated by SDS–polyacrylamide gel electrophoresis (SDS–PAGE) and subjected to Western blot analysis with anti-HA (Clontech Laboratories, Palo Alto, CA, USA) or anti-FLAG antibodies (M2, Sigma-Aldrich, Inc., St Louis, MO, USA). Immunoreactive bands

were visualized using a chemiluminescent reagent (ECL-PLUS Western blotting detection kit, GE Healthcare) and X-ray films. ImageJ (NIH) was used to measure the densities of immunoreactive bands and statistical analysis was performed using Student's *t*-test.

Transferrin incorporation

HeLa cells were transfected with pcDNA3-Arf6(Q67L)-FLAG or pCAGGS-FLAG-synArfGEF plus pcDNA3-Arf6-HA using Lipofectamine 2000. One day after transfection, cells were serum-starved for 3 h and incubated with Alexa488-conjugated transferrin (25 μg/mL) for 20 min at 37°C. The cells were then fixed with 4% paraformaldehyde and immunostained with anti-FLAG IgG. Fluorescent images and intensities were acquired using a confocal microscope (TCS SP2 AOBS, Leica Microsystems, Wetzlar, Germany). The fluorescent intensities of cytoplasmic transferrin in transfected cells were statistically compared with those in non-transfected cells observed in the same fields using Scheffe's test. Three independent experiments were performed.

Antibodies

The fusion proteins of GST and maltose-binding protein to synArfGEF, gephyrin, S-SCAM, or utrophin were expressed in *Escherichia coli* BL21 (DE3) (Stratagene) in the presence of 1 mM isopropyl β D-thiogalactopyranoside and purified with glutathione-Sepharose 4B and amylose-resin (New England Biolabs), respectively. These GST fusion proteins were then used to immunize rabbits and guinea pigs. The antibodies were affinity-purified with CNBr-activated Sepharose (GE Healthcare) coupled with respective maltose-binding protein fusion proteins. The specificity of antibodies for gephyrin, S-SCAM, utrophin was characterized by Western blot analysis (Figure S1).

Western blot analysis

Mouse brains and COS-7 cells transfected with pCAGGS-FLAG-synArfGEF, pCAGGS-FLAG-IQ-ArfGEF/BRAG1 or pCAGGS-FLAG-GEP100 were homogenized with a buffer containing 125 mM Tris–HCl, pH 6.8, 4% SDS, 20% glycerol, 1% sodium deoxycholate, 10% β-mercaptoethanol and a cocktail of protease inhibitors (Complete Mini™, Roche) and boiled for 5 min. After centrifugation, the lysates were separated by SDS–PAGE and transferred onto polyvinyl difluoride membranes (PVDF-PLUS, Micron Separations Inc., Westborough, MA, USA). The membranes were incubated with antibodies against synArfGEF (0.5 μg/mL) or FLAG (M2, Sigma-Aldrich, 0.5 μg/mL) and subsequently with peroxidase-conjugated secondary antibodies. Immunoreactive bands were visualized using a chemiluminescent reagent (ECL-PLUS Western blotting detection kit, GE Healthcare).

Immunostaining

To confirm the specificity of antibodies, COS-7 cells were plated onto 35-mm dishes at the density of 2×10^5 per dish and transfected with pCAGGS-FLAG-synArfGEF, pCAGGS-FLAG-IQ-ArfGEF/BRAG1 or pCAGGS-FLAG-GEP100 using Lipofectamine 2000 (Invitrogen). Twenty-four hours after transfection, cell were fixed with 4% paraformaldehyde and subjected to double immunostaining with antibodies against synArfGEF and FLAG epitope.

Under deep anesthesia with diethyl ether, C57BL/6N male mice at postnatal 10–12 weeks transcardially fixed with 4% paraformaldehyde plus 0.2% picric acid in 0.1 M phosphate buffer (pH 7.4). Brains were further immersed with the same fixative overnight, cryoprotected in 30% sucrose, and sliced at a thickness of 30 μm with a cryostat. Hippocampal cultures were prepared from 18-day-old rat embryos at the plating density of 0.6×10^6 per 35-mm dish as described previously (Sakagami *et al.* 2005). At 22 days *in vitro*, plates were fixed with 2% paraformaldehyde for 5 min.

For immunoperoxidase staining, brain sections were solubilized in 0.3% Triton X-100 for 30 min, blocked with 5% normal goat serum for 30 min, and incubated with anti-synArfGEF IgG (1 μg/mL) overnight. After washing extensively with phosphate-buffered saline, they were subsequently incubated with peroxidase-conjugated anti-rabbit IgG (Histofine Simple Stain MAX PO (R) kit, Nichirei, Tokyo, Japan) for 1 h at 23°C. Immunoreactions were visualized with 3,3′-diaminobenzidine tetrahydrochloride chromogenic substrate (Liquid DAB and Substrate Chromogen System, K3468; DAKO, Tokyo, Japan). The pre-embedding silver-enhancement immunogold method was described previously (Sakagami *et al.* 2008). Briefly, after incubation with the primary antibody, the sections were incubated with nanogold-conjugated anti-rabbit IgG (1 : 100, Nanoprobes Inc., Yaphank, NY, USA), washed with phosphate-buffered saline, and fixed with glutaraldehyde for 10 min. The gold labeling was intensified for 3–5 min under a safety red light using a HQ Silver Enhancement kit (Nanoprobe Inc.) according to the manufacturer's instructions. The sections were treated with 1% osmium tetroxide and 2% uranyl acetate, dehydrated with ethanol and embedded in epoxy resin. Ultrathin sections were examined with a JEM-1230 electron microscope (JEOL Ltd., Tokyo, Japan).

For immunofluorescent staining, samples were incubated with the combination of rabbit or guinea pig polyclonal anti-synArfGEF IgG with guinea pig anti-gephyrin IgG, guinea pig anti-PSD-95 IgG (Fukaya and Watanabe 2000), rabbit anti-IQ-ArfGEF/BRAG1 (Sakagami *et al.* 2008), rabbit $GABA_AR$ α1 subunit IgG (Alamone Labs, Jerusalem, Israel), anti rabbit anti-vesicular GABA transporter (VGAT) (Fukudome *et al.* 2004), guinea pig anti-α-amino-3-hydroxy-5-methyl-4-isoxazolepropionate-type glutamate receptor GluA2 subunit IgG (Yamazaki *et al.* 2010), guinea pig anti-S-SCAM IgG, mouse monoclonal anti-glycine receptor α1 subunit IgG (clone mAb4a, Synaptic Systems, Gottingen, Germany) or anti-dystrophin IgG (MANDRA-1, Sigma). Immunoreactions were visualized with the appropriate combination of the following secondary antibodies: Alexa488-conjugated anti-rabbit IgG, Alexa488- or Alexa594-conjugated anti-guinea pig IgG, and Alexa594- or Alexa647-conjugated anti-mouse IgG (Molecular Probes, Inc., Eugene, OR, USA). Nuclei were counter-stained with 4′,6-diamidino-2-phenylindole dihydrochloride. Immunofluorescent images were taken with a confocal microscope (LSM 710, Carl Zeiss, Oberkochen, Germany) using ×20 and ×63 plan-apochromat objective lens. The brightness and contrast of the final images were adjusted using Photoshop CS4 software (Adobe Systems, San Jose, CA, USA). In control experiments, the primary antibody was pre-incubated with the antigen (10 μM) before immunostaining.

Yeast two-hybrid assay

Yeast two-hybrid screening was performed as described previously (Sakagami *et al.* 2007, 2008). Briefly, approximately 2×10^6 clones of a mouse brain cDNA library were screened using pDBLeu-

synArfGEF(1122–1194), which encoded the fusion protein of C-terminal 73 amino acids of rat synArfGEF to the GAL4 DNA-binding domain, by the ability to grow on selective medium lacking histidine, leucine and tryptophan supplemented with 10 mM 3-aminotriazole. Positive colonies were further selected by the β-galactosidase assay and uracil prototrophy. Plasmids were subjected to the sequencing analysis. To verify the interaction, the yeast strain MaV203 was co-transformed with the indicated combination of bait pDBLeu and prey pPC86 vectors shown in Figs 6 and 7. The interactions were tested by the β-galactosidase assay and the ability to grow without histidine and uracil.

In vitro binding assay

COS-7 cells were transiently transfected with various plasmid constructs encoding myc-tagged S-SCAM or FLAG-synArfGEF and lysed in the lysis buffer consisting of 50 mM Tris-HCl (pH 7.5), 150 mM NaCl, 1% Nonidet P-40 and a cocktail of protease inhibitors (Complete Mini™, Roche). Lysates were incubated with 15 μg of GST, GST-synArfGEF 1122–1194, GST-utrophin 2691–3429, 2691–3058, 2691–2843, 2937–3685, or GST-dystrophin 2937–3685, immobilized on glutathione-Sepharose 4B for 1 h at 4°C. Afterwards, the beads were washed five times with the lysis buffer containing 150 mM or 300 mM NaCl and the proteins were eluted with SDS sample buffer. The cell lysates and eluates were analyzed by Western blot analysis with anti-myc IgG or anti-FLAG IgG.

For pull down assays from brain extracts, mouse brains were homogenized with 10 volumes of the lysis buffer and centrifuged at 12 000 *g* for 15 min. The supernatant (1 mg) were pre-cleaned with glutathione-Sepharose 4B for 30 min and incubated with 20 μg of GST, GST-utrophin 2691–3429, or GST-dystrophin 2937–3685, which were immobilized on glutathione-Sepharose 4B, for 1 h at 4°C. The precipitates were washed with the lysis buffer containing 150 or 300 mM NaCl and subjected to Western blot analysis with rabbit anti-synArfGEF IgG.

Immunoprecipitation

Immunoprecipitation from brain lysates was performed as described previously (Sakagami *et al.* 2008). Briefly, the mouse brain P2 fraction was solubilized with 1% sodium deoxycholate in 50 mM

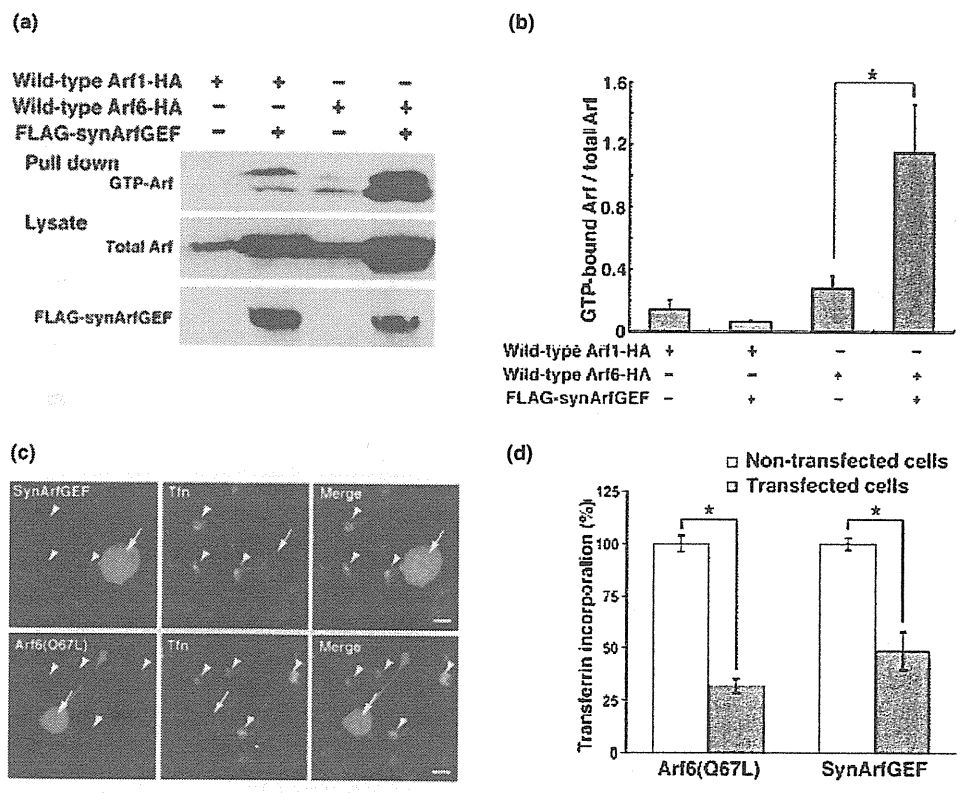

Fig. 1 SynArfGEF activates Arf6. (a) Arf pull down assays. COS-7 cells were transfected with the indicated combination of vectors and were subjected to Arf pull down assays with the GST-GGA1 fusion protein. (b) Quantification of the ratio of GTP-bound Arfs to total Arfs. Note the significant increase in GTP-Arf6 in the presence of FLAG-synArfGEF ($p < 0.01$, Student's *t*-test). Data are represented as mean ± SD from three independent transfection samples. (c) Transferrin incorporation assay. HeLa cells were transfected with FLAG-synArfGEF plus Arf6-HA or Arf6(Q67L)-FLAG. After serum-starvation, cells were incubated with Alexa488-transferrin and subjected to immunostaining. Representative figures show the decreased transferrin incorporation in cells expressing FLAG-synArfGEF and Arf6-HA or Arf6(Q67L)-FLAG (arrows) compared with that in non-transfected cells (arrowheads). Scale bars, 10 μm. (d) Quantification of the fluorescence intensity of intracellular transferrin. Data are represented as mean ± SEM from three independent experiments. Asterisks indicate significant difference of fluorescence intensities between transfected and non-transfected cells ($p < 0.01$, Scheffe's test).

Tris–HCl (pH 9.0) and dialyzed against the binding buffer [0.1% Triton X-100, 50 mM Tris–HCl (pH 7.4)]. After pre-cleaning with Protein G-Sepharose 4B, the soluble supernatant (1 mg) was incubated with 5 μg of anti-synArfGEF IgG or normal rabbit IgG for 1 h at 4°C and with Protein G-sepharose 4B for another 1 h. The beads were washed five times with the binding buffer plus 150 mM NaCl. Proteins were eluted with SDS sample buffer, subjected to SDS–PAGE and immunoblotted with antibodies against S-SCAM (M2441, Sigma) or β-dystroglycan (clone 43DAG1/8D5, Novacastra Laboratories, Newcastle, UK).

Results

SynArfGEF activates Arf6

Two related proteins in the BRAG/IQSEC family of Arf-GEFs, IQ-ArfGEF/BRAG1/IQSEC2 and GEP100/BRAG2/IQSEC1 have previously been shown to activate Arf6 (Someya *et al.* 2001; Sakagami *et al.* 2008). To examine whether synArfGEF/BRAG3/IQSEC3 activates Arf6, we performed Arf pull down assays with a GST-GGA1 fusion protein that is capable of binding GTP-bound Arfs of all classes. COS-7 cells were co-transfected with FLAG-synArfGEF and Arf1-HA or Arf6-HA. Immobilized GST-GGA1 pulled down 4.13-fold more GTP-Arf6-HA from the lysates of COS-7 cells expressing both Arf6-HA and FLAG-synArfGEF than Arf6-HA alone ($p = 0.0092$ by Student's *t*-test, Fig. 1a and b). Co-transfection of Arf1-HA and FLAG-synArfGEF increased both total and GTP-bound Arf1 to a similar extent and did not change the ratio of GTP-Arf1 to total Arf1 (Fig. 1a and b). We further examined the ability of synArfGEF to activate Arf6 *in vivo* using a transferrin incorporation assay. Arf6 has been shown to regulate the endocytosis of transferrin receptor (D'Souza-Schorey *et al.* 1995). If synArfGEF activates Arf6 *in vivo*, transferrin uptake would be affected by over-expressing synArfGEF. We therefore examined the incorporation of transferrin in HeLa cells transfected with FLAG-synArfGEF and Arf6-HA. In non-transfected cells, transferrin accumulated in the perinuclear region (Fig 1c). By contrast, the incorporation of transferrin was reduced by 48.7% in cells transfected with FLAG-synArfGEF and Arf6-HA compared to non-transfected cells (Fig. 1c and d). This reduction was comparable with the reduction (31.9%) observed for cells transfected with the GTP hydrolysis-defective Arf6 mutant, Arf6(Q67L). Taken together, these findings suggest that synArfGEF activates Arf6 *in vivo*.

Preferential localization of synArfGEF at inhibitory synapses

We have previously shown that synArfGEF mRNA is expressed preferentially in the olfactory bulb, cerebral cortex, hippocampus, brainstem nuclei and cerebellar Purkinje cells of the adult rat brain (Inaba *et al.* 2004). In this study, we produced novel anti-synArfGEF antibodies for use in immunohistochemistry. Western blot analysis using the lysates of COS-7 cells transfected with FLAG-tagged BRAG family members showed that both antibodies raised in rabbit and guinea pig detected FLAG-synArfGEF, while they did not cross-react with other BRAG members, FLAG-IQ-ArfGEF/BRAG1 or GEP100 (Fig. 2). In the mouse brain lysate, the antibodies gave two immunoreactive bands of 160 and 130 kDa (Fig. 2), suggesting the existence of two alternatively spliced isoforms as is the case for the other BRAG/IQSEC family members (Dunphy *et al.* 2006; Shoubridge *et al.* 2010). Notably, the electrophoretic mobility of the 160 kDa band was consistent with that of recombinant FLAG-synArfGEF detected using an anti-FLAG antibody (Fig. 2). Further to confirm the specificity, COS-7 cells were transfected with FLAG-tagged BRAG members and subjected to immunostaining. Again, the antibodies specifically detected COS-7 cells transfected with FLAG-synArfGEF without any immunolabeling in non-transfected cells or cells transfected with FLAG-IQ-ArfGEF/BRAG1 or GEP100 (Figure S2). Immunoperoxidase staining of mouse brain sections with rabbit anti-synArfGEF IgG yielded intense labeling in the olfactory bulb, cerebral cortex, hippocampal formation, reticular thalamic nucleus, superior and inferior colliculi, cerebellar cortex and various brainstem nuclei (Fig. 3a). This immunolabeling pattern was compatible with the expression pattern of synArfGEF mRNA in the rat brain described previously (Inaba *et al.* 2004). In control experiments, the primary antibody pre-absorbed with the antigen did not show any immunolabeling (Fig. 3b). In addition, both rabbit and guinea pig antibodies gave an identical labeling pattern (data not shown). Taken together, all these

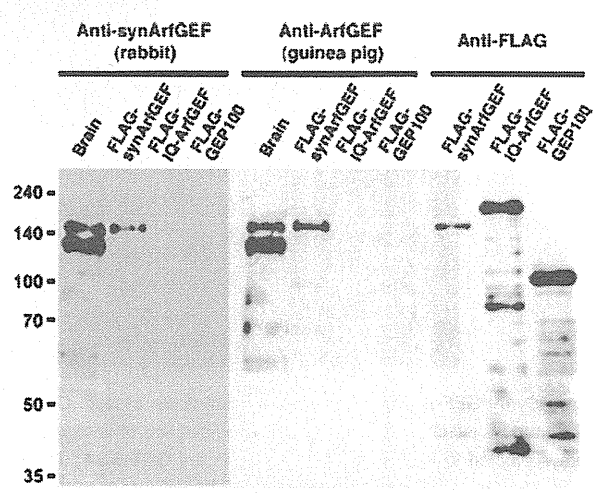

Fig. 2 Characterization of anti-synArfGEF antibodies by Western blot analysis. Lysates from mouse brain and COS-7 cells expressing FLAG-tagged synArfGEF, IQ-ArfGEF/BRAG1, or GEP100 were subjected to Western blot analysis with rabbit and guinea pig polyclonal antibodies against synArfGEF or anti-FLAG IgG.

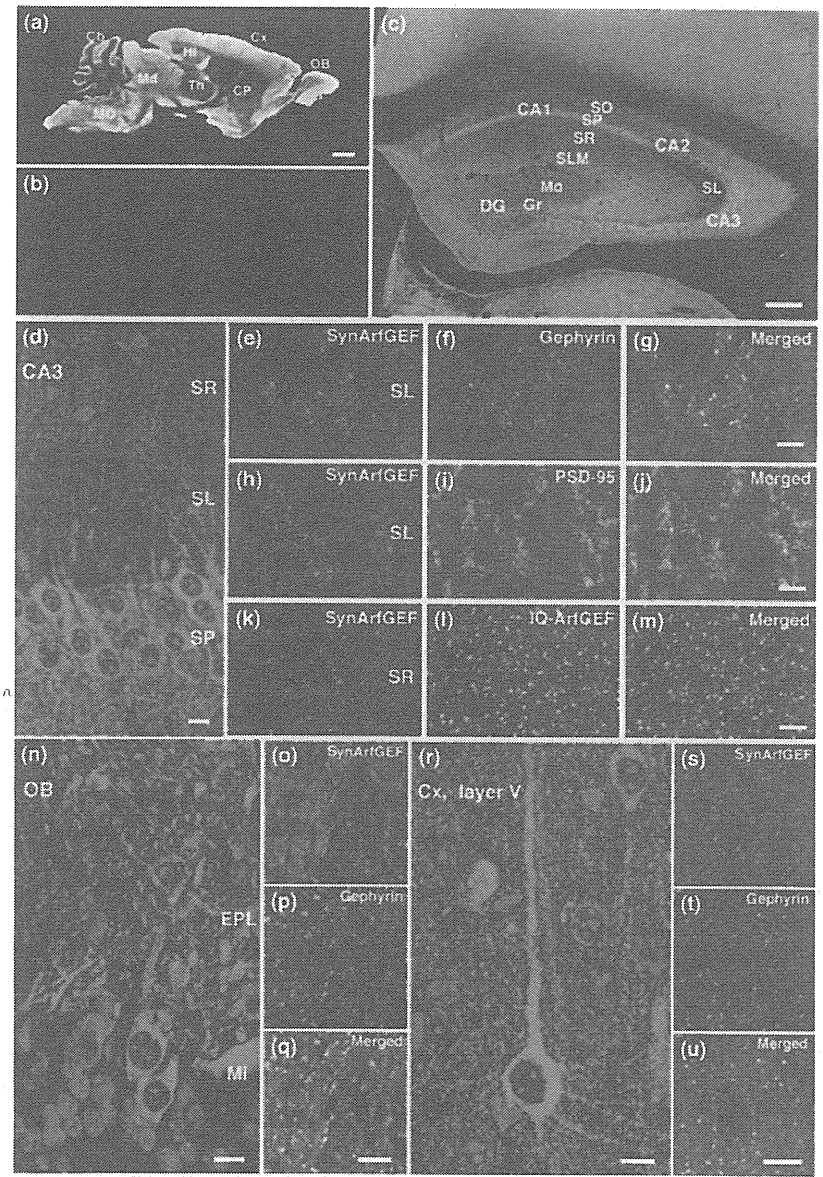

Fig. 3 Immunohistochemical localization of synArfGEF in the forebrain. (a, b) Sagittal sections from adult mouse brain were subjected to immunoperoxidase staining with the rabbit polyclonal anti-synArfGEF IgG (a) or antibody pre-absorbed with the antigen (10 μM) (b). Note the complete attenuation of immunolabeling by pre-incubation with the antigen. (c) Immunofluorescent localization of synArfGEF in the adult mouse hippocampus. (d–m) Immunofluorescent localization of synArfGEF in the hippocampal CA3 region. Coronal sections were immunostained for synArfGEF (e, h, k) and gephyrin (f), PSD-95 (i), or IQ-ArfGEF/BRAG1 (l). Note the colocalization of synArfGEF with gephyrin but not PSD-95 or IQ-ArfGEF. (n–q) Immunofluorescent localization of synArfGEF in the olfactory bulb. Note the colocalization of synArfGEF (o) and gephyrin (p) in the external plexiform layer (EPL). (r–u) Immunofluorescent localization of synArfGEF in the cerebral pyramidal neurons. Note the colocalization of synArfGEF (s) and gephyrin (t). Nuclei were counter-stained with 4′,6-diamidino-2-phenylindole dihydrochloride (DAPI) (blue) in panles d, n, and r. CA1-3, subfield CA1-3 of Ammon's horn; Cb, cerebellar cortex; CP, caudate putamen; Cx, cerebral cortex; DG, dentate gyrus; Gr, dentate granule cell layer; Hi, hippocampus; Md, midbrain; Mi, mitral cell layer; MO, medulla oblongata; Mo, molecular layer, OB, olfactory bulb; SL, stratum lucidum; SLM, stratum lacunosum-moleculare; SO, stratum oriens; SP, stratum pyramidale; SR, stratum radiatum; Th, thalamus. Scale bars, 1 mm (a); 200 μm (c); 10 μm (d, n, R); 5 μm (g, j, m, q, u).

findings suggest the immunolabeling observed with these antibodies is specific for synArfGEF.

In the hippocampus, synArfGEF immunoreactivity was widely distributed, with the highest level observed in the CA3 region (Fig. 3c). SynArfGEF labeling was observed diffusely in both neuronal somata and dendrites, but not in nuclei, of pyramidal cells. In addition to this diffuse cytoplasmic labeling, tiny puncta (< 1 μm in diameter) were distributed on the surface of the somata and dendrites (Fig. 3d), consistent with synaptic localization. To examine whether synArfGEF is associated with excitatory or inhibitory synapses, double immunofluorescence staining was performed with antibodies against synArfGEF and PSD-95, gephyrin or IQ-ArfGEF/BRAG1 (Fig. 3e–m). Extensive colocalization was observed between synArfGEF and gephyrin along somata and dendritic shafts (Fig. 3e–g), whereas synArfGEF puncta were rarely co-localized with PSD-95 or IQ-ArfGEF/BRAG1 (Fig. 3h–m).

In the olfactory bulb, synArfGEF immunoreactivity was distributed in the mitral cell, external plexiform, and glomerular layers (Fig. 3n). In mitral cells, somata and dendrites were heavily immunolabeled. Along their dendritic shafts in the external plexiform layer, synArfGEF labeling was distributed as puncta largely co-localized with gephyrin (Fig. 3o–q).

In the neocortex, synArfGEF immunoreactivity was distributed throughout the cortical layers. Pyramidal neurons in the layer V were intensely immunolabeled in their somatodendritic compartments without nuclear staining

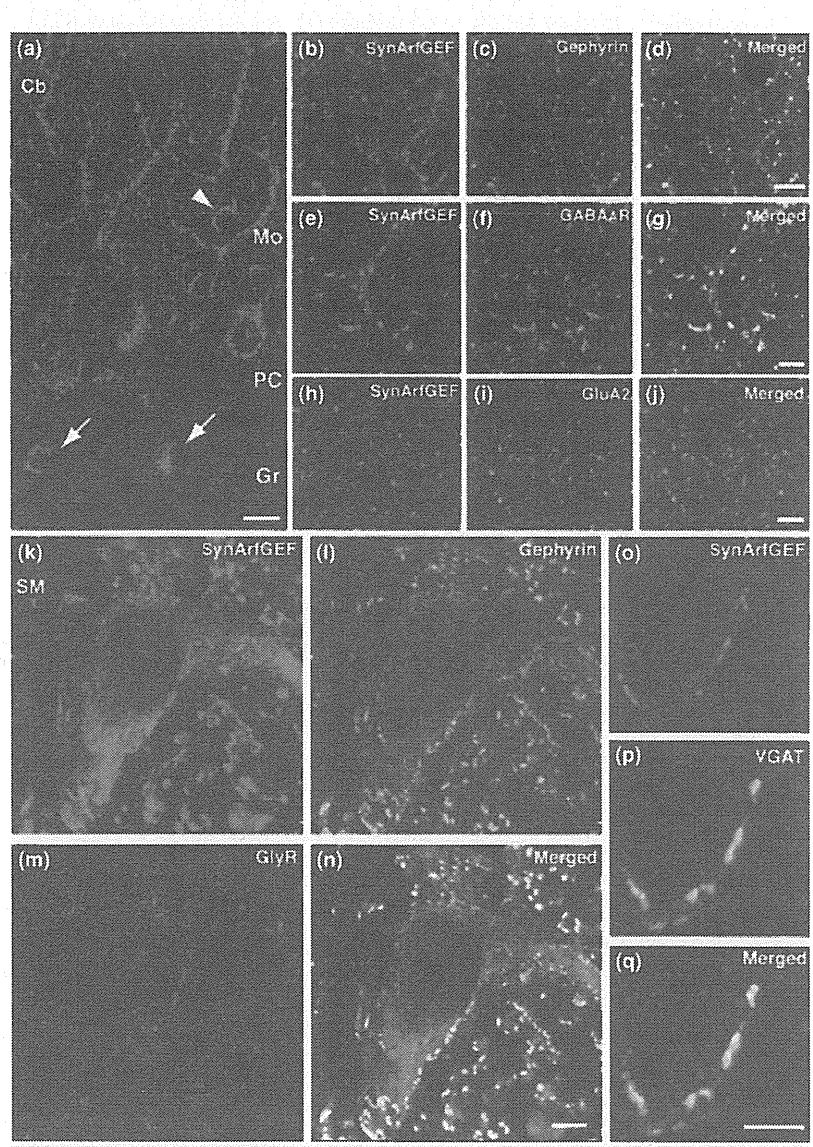

Fig. 4 Immunohistochemical localization of synArfGEF in the cerebellum and spinal cord. (a–j) Localization of synArfGEF in the cerebellar cortex (Cb). A sagittal section of the adult mouse cerebellar cortex (Cb) was immunostained for synArfGEF (b, e, h) and gephyrin (c), $GABA_AR$ α1 subunit (f), or GluA2 subunit (i). Note that immunolabeling of synArfGEF in the cell bodies of Purkinje cells, basket cells (arrowhead), stellate cells and Golgi cells (arrows) as well as dendrites of Purkinje cells in the molecular layer (Mo). Also note the colocalization of synArfGEF with gephyrin and $GABA_AR$ α1 subunit but not GluA2 subunit in the molecular layer. Gr, granular layer; PC, Purkinje cell layer. (k–q) Localization of synArfGEF in spinal motoneurons (SM). Coronal sections of the spinal cord were immunostained for synArfGEF (k), gephyrin (l) and glycine receptor α subunit (m) or with synArfGEF (o) and VGAT (p). Note the colocalization of synArfGEF, gephyrin and glycine receptor α subunit along the cell body/dendritic shafts and the close apposition of synArfGEF to VGAT. Scale bar, 20 μm (a); 5 μm (d, g, j, n, q).

(Fig. 3r). At high magnification, synArfGEF was found in fine puncta along the somata and dendrites, which were largely co-localized with gephyrin (Fig. 3s–u).

In the cerebellar cortex, synArfGEF immunoreactivity was observed in the somata and dendritic shafts of Purkinje cells, and the somata of basket cells and stellate cells in the molecular layer, and the somata of Golgi cells in the granular layer (Fig. 4a). However, the somata of granule cells were devoid of immunolabeling for synArfGEF. At high magnification, tiny immunoreactive puncta were found to be distributed along Purkinje cell dendrites and co-localized well with gephyrin (Fig. 4b–d) and $GABA_AR$ α1 subunit (Fig. 4e–g) without overlapping with α-amino-3-hydroxy-5-methyl-4-isoxazolepropionate receptor GluA2 subunit (Fig. 4h–j).

In the spinal cord, synArfGEF immunoreactivity was distributed in the gray matter. In particular, the somata and dendrites of ventral motoneurons were heavily immunolabeled (Fig. 4k). The immunoreactive puncta along the somata and dendritic shafts were largely co-localized with both glycine receptors and gephyrin (Fig. 4k–n). Immunoreactive puncta were also closely apposed to VGAT labeling, forming merged color at the interface (Fig. 4o–q). These confocal microscopic results suggest that synArfGEF is preferentially distributed at inhibitory synapses throughout the central nervous system.

To determine the precise synaptic localization, we performed pre-embedding immunogold electron microscopy in the external plexiform layer of the olfactory bulb (Fig. 5a), the molecular layer of the cerebellar cortex (Fig. 5b), and spinal motoneurons (Fig. 5c). Immunogold particles for synArfGEF accumulated on or beneath the post-synaptic membrane of symmetric synapses formed on dendritic shafts

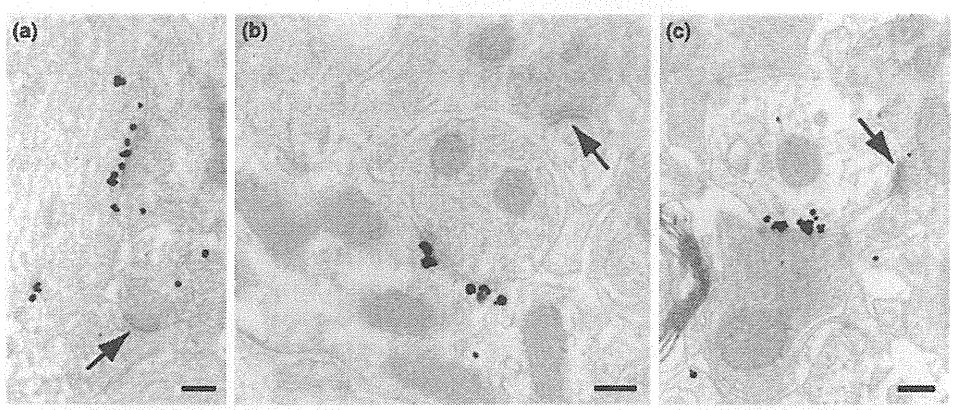

Fig. 5 Subcellular localization of synArfGEF by immunoelectron microscopy using the silver-enhanced immunogold method. Note the accumulation of immunogold particles for synArfGEF at post-synaptic specializations of symmetric synapses of the dendritic shafts of an olfactory mitral cell in the external plexiform layer (a), a Purkinje cell in the molecular layer (b), and a spinal motoneuron (c). Note the absence of immunolabeling at asymmetric synapses (arrows). Scale bars, 200 nm.

and cell bodies. By contrast, no significant immunogold particles were observed at asymmetric synapses on olfactory mitral cells (Fig. 5a), cerebellar Purkinje cells (Fig. 5b), or spinal motoneurons (Fig. 5c). These findings confirm that synArfGEF localizes exclusively at post-synaptic specializations of inhibitory synapses.

Interaction of synArfGEF with utrophin/dystrophin

To identify interacting proteins with synArfGEF, we performed yeast two-hybrid screening of a mouse brain cDNA library, using the C-terminal 73 amino acids of synArfGEF as bait. We isolated two independent cDNA clones (#5 and #57) encoding utrophin, a large cytoskeletal protein with high structural similarity to dystrophin (Fig. 6a). Both clones encoded an overlapping C-terminal region (amino acids 2698–3429) containing a partial 20th spectrin repeat, the WW and Zn^{2+} finger motifs, and two coiled-coil domains. As dystrophin was shown to localize at inhibitory synapses and to regulate the clustering of selected $GABA_AR$ subtypes (Knuesel *et al.* 1999), we further examined whether the corresponding C-terminal region of dystrophin (amino acids 2937–3685) could interact with the C-terminus of synArfGEF. Indeed, yeast expressing dystrophin 2937–3685 and synArfGEF 1122–1194 exhibited significant β-galactosidase activity and the ability to grow without histidine and uracil (Fig. 6b), indicating a robust protein-protein interaction. Next, we determined the region of utrophin responsible for the interaction with synArfGEF using two-hybrid assays with synArfGEF bait and various truncated mutants of utrophin as shown in Fig 6a. Yeast expressing synArfGEF and utrophin fragments 2691–3429, 2691–3111 and 2691–3058 exhibited detectable β-galactosidase activity, although the prototrophy for histidine and uracil was markedly disturbed in yeast expressing utrophin 2691–3111 and 2691–3058 (Fig. 6b). The interaction was not detected when utrophin 2691–3058 was further truncated (amino acids 2810–3058, 2691–2843, or 2810–2843) or the WW motif was deleted (utrophin fragments 2843–3429, 3061–3429, and 3249–3429) (Fig. 6a). These findings suggest that the minimal region of utrophin required for the interaction corresponds to amino acids 2691–3058.

The synArfGEF-utrophin interaction was also independently verified using pull down assays. Consistently, GST-utrophin 2691–3429, 2691–3058 and GST-dystrophin 2937–3685 were capable of efficient pull down of full-length FLAG-synArfGEF from transfected COS-7 cell lysates, whereas neither GST-utrophin 2691–2843 nor GST alone was capable of mediating this interaction (Fig. 6c). The synArfGEF-utrophin interaction was retained even when the salt concentration in the washing buffer was raised to 300 mM, although the interaction between GST-utrophin 2691–3058 and synArfGEF was decreased (Fig. 6c). Furthermore, GST-utrophin 2691–3429 and GST-dystrophin 2937–3685, but not GST alone, efficiently pulled down endogenous synArfGEF from brain extracts (Fig. 6d).

The C-terminal 73 amino acids of synArfGEF used as bait contain a proline-rich sequence and type I PDZ-binding motif. The proline-rich domain is followed by a tyrosine residue (sequence PPPPY), which forms a known motif for binding to WW domains – the PY motif (Chen and Sudol 1995; Rentschler *et al.* 1999) (Fig. 7a). As the minimal region of utrophin required for robust interactions with synArfGEF contains a WW motif, we examined whether this PY motif mediated the synArfGEF–utrophin interaction. Activation of reporter genes was observed when yeast was co-transformed with utrophin 2653–3429 and synArfGEF 1122–1194, ΔC3, 1122–1172, or 1141–1194, all of which contained the PY motif, although the β-galactosidase activity was dramatically reduced in the yeast transformed with

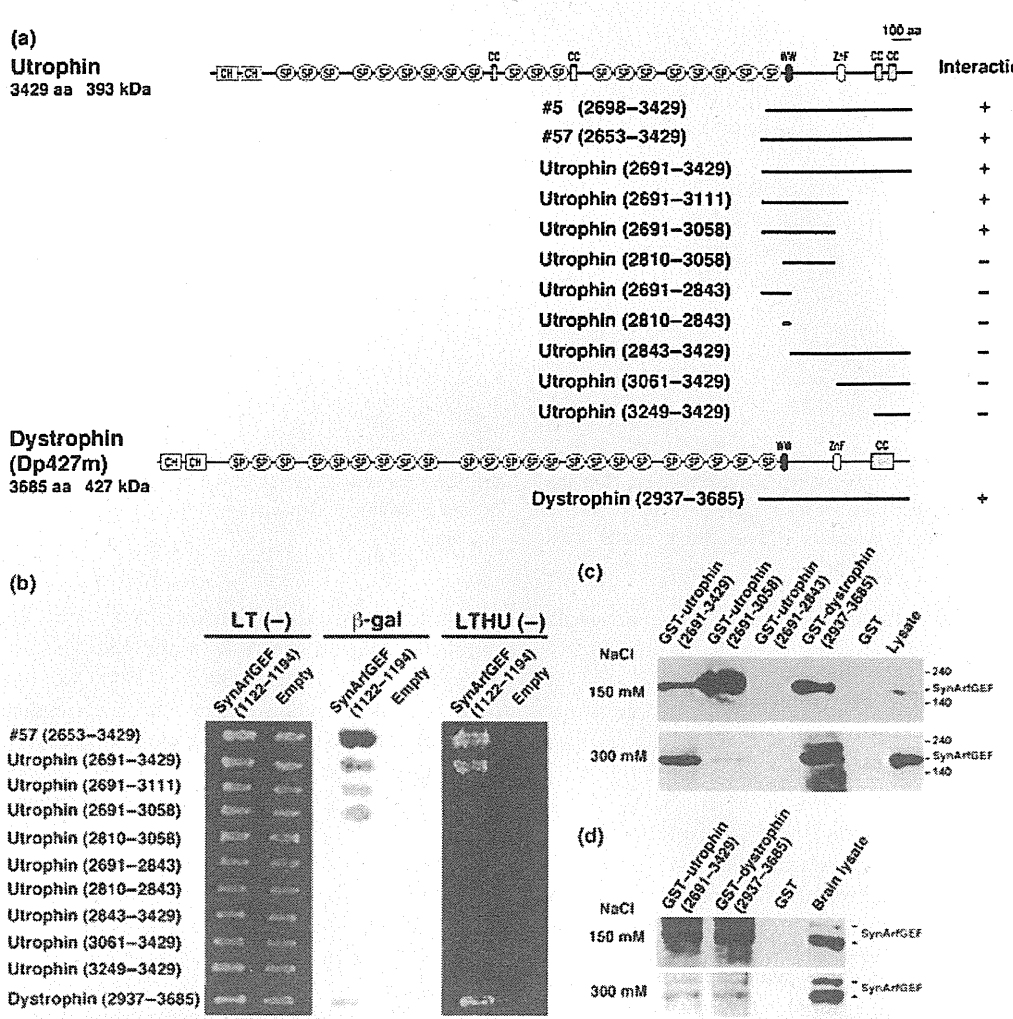

Fig. 6 Interaction of synArfGEF with utrophin/dystrophin. (a) Schematic representation of the domain structures of utrophin and dystrophin and the protein fragments used in the yeast two-hybrid assays. (b) Two-hybrid assays. The yeast strain MaV203 was transformed with the indicated combinations of constructs and plated onto synthetic complete medium lacking leucine and tryptophan: LT(–), or leucine, tryptophan, histidine and uracil: LTHU(–). Interactions were assessed by β-galactosidase activity (β-gal) and prototrophy for histidine and uracil. Note the interaction of synArfGEF with utrophin fragments 2653–3429, 2691–3429, 2691–3111, 2691–3058, and dystrophin fragment 2937–3685. (c, d) Pull down assays. Lysates from COS-7 cells transfected with pCAGGS-FLAG-synArfGEF (c) and mouse brains (d) were subjected to pull down assays with the indicated GST fusion proteins that were conjugated with glutathione-Sepharose 4B. The precipitates were washed with the lysis buffer containing 150 or 300 mM NaCl and subjected to Western blot analysis with anti-FLAG IgG (c) or anti-synArfGEF IgG (d).

utrophin 2653–3429 and synArfGEF 1122–1172 (Fig. 7b). The substitution of proline and tyrosine residues in the PY motif to alanine residues (PPPPY → PPAPA) disrupted the interaction between synArfGEF and utrophin (Fig. 7a and b), suggesting that the PY motif in synArfGEF is critical for this interaction.

To examine whether synArfGEF and utrophin/dystrophin co-localize at synapses, cultured hippocampal neurons were prepared from rat embryos, maintained for 22 days and immunostained with antibodies against synArfGEF and dystrophin or utrophin. Dendritic synArfGEF puncta showed extensive colocalization with dystrophin (Fig. 8b–d). By contrast, anti-utrophin did not immunolabel hippocampal neurons (data not shown). Furthermore, synArfGEF-immunoreactive puncta were also associated with $GABA_AR$ α1 subunit and VGAT but not with PSD-95 (Fig. 8e–m). Taken together, these findings suggest that synArfGEF and dystrophin form a complex at inhibitory synapses of hippocampal neurons *in vivo*, mediated by PY-motif and WW domain interactions.

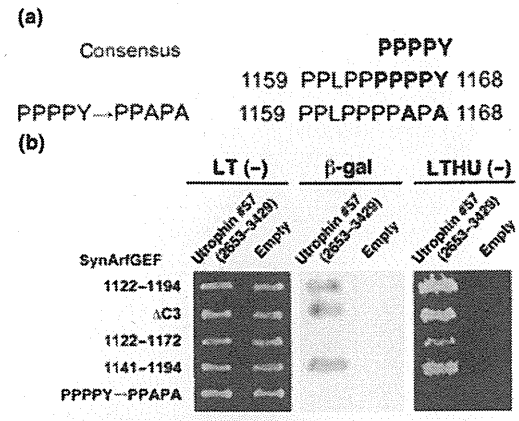

Fig. 7 Interaction of synArfGEF with utrophin via a PPPPY motif. (a) Sequence alignment of the consensus PPPPY motif required for binding to WW domains, proline-rich sequence of the C-terminal region of synArfGEF and the mutant (PPPPY → PPAPA). (b) Two-hybrid assays. The yeast strain MaV203 was transformed with the indicated combinations of constructs and plated onto synthetic complete medium lacking leucine and tryptophan: LT(−) or leucine, tryptophan, histidine and uracil: LTHU(−). Interactions were assessed by β-galactosidase activity (β-gal) and the ability to grow on LTHU(−) medium. Note the disruption of the interaction with utrophin by the mutation in a PPPPY motif (PPPPY → PPAPA).

Interaction of synArfGEF with S-SCAM/MAGI-2

In addition to utrophin, we also isolated several independent clones encoding the membrane-associated guanylate kinase with inverted orientation (MAGI) family, which contains six PDZ domains, two WW domains and one guanylate kinase domain and comprises of three members, MAGI-1, S-SCAM (also called MAGI-2), and MAGI-3. S-SCAM was previously shown to localize at inhibitory synapses and to act as a molecular bridge between the neurexin-neuroligin complex and the DGC via direct interactions with two adhesion molecules at inhibitory synapses, neuroligin-2 and β-dystroglycan (Sumita *et al.* 2007). We therefore examined whether synArfGEF could interact with S-SCAM using pull down assays (Fig. 9a). GST-synArfGEF 1122–1194 efficiently pulled down full-length S-SCAM from lysates of transfected COS-7 cells. We further determined which region of S-SCAM was responsible for this interaction using various truncated S-SCAM mutants as shown in Fig. 9a. GST-synArfGEF 1122–1194 could efficiently pull down S-SCAM 295–578 containing two WW domains and the PDZ1 domain, while it could not pull down S-SCAM 1–301 or 573–1277. Although the binding efficiency was drastically reduced, S-SCAM 425–578 containing only PDZ1 domain retained the ability to bind to GST-synArfGEF 1122–1194 (Fig. 9a), indicating that PDZ1 domain is the minimal requirement for the interaction with synArfGEF.

To examine whether synArfGEF co-localizes with S-SCAM at synapses, we performed double immunofluorescent staining of the cerebellar cortex (Fig. 9b). In the molecular layer, both synArfGEF and S-SCAM were distributed in puncta, although S-SCAM puncta were slightly larger in size. The anti-synArfGEF IgG labeled 43% of S-SCAM puncta (n = 202), whereas the anti-S-SCAM IgG labeled 26% of synArfGEF puncta (n = 335). These findings suggest that synArfGEF partially co-localizes with S-SCAM in the cerebellar molecular layer.

Finally, we performed co-immunoprecipiation experiments from brain lysates to examine whether synArfGEF forms a proteins complex with dystrophin and S-SCAM *in vivo*. The anti-synArfGEF IgG, but not normal rabbit IgG, efficiently immunoprecipitated S-SCAM from the deoxycholate-solubilized P2 fraction (Fig. 9c). Although we failed to detect dystrophin or utrophin in the immunoprecipitates (data not shown), the anti-synArfGEF IgG clearly immunoprecipitated

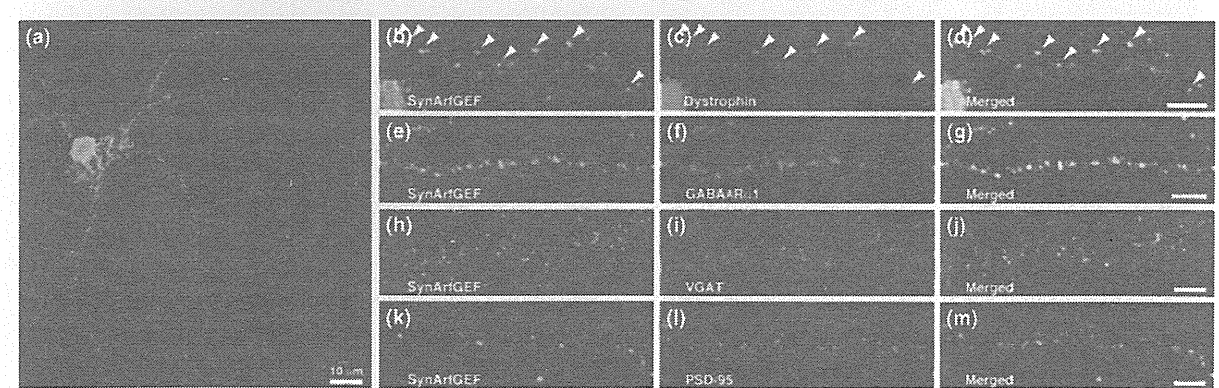

Fig. 8 Colocalization of synArfGEF and dystrophin at inhibitory synapses of cultured hippocampal neurons. Cultured hippocampal neurons at 22 DIV were immunostained with anti-synArfGEF (a, b, e, h, k) and anti-dystrophin (c), $GABA_AR$ α1 subunit (f), VGAT (i) or PSD-95 (l) antibodies. Note the close association of synArfGEF with dystrophin, $GABA_AR$ α1 and VGAT but not with PSD-95. Arrowheads in high-magnification views (b–d) show the colocalization of endogenous synArfGEF and dystrophin along dendrites. Scale bars, 10 μm (a); 5 μm (d, g, j, m).